

# Highly Supercritical Convection in Strong Magnetic Fields

by

Keith Julien<sup>1</sup>, Edgar Knobloch<sup>2</sup> and Steve Tobias<sup>3</sup>

<sup>1</sup> Department of Applied Mathematics, University of Colorado, Boulder CO  
80309

<sup>2</sup> Department of Physics, University of California, Berkeley CA 94720

<sup>3</sup> Department of Applied Mathematics and Theoretical Physics, University of  
Cambridge, Cambridge, CB3 9EW, UK

## Abstract

Fully nonlinear convection in a strong imposed magnetic field is studied in the regime in which the convective velocities are not strong enough to distort the magnetic field substantially. Motivated by convection in sunspots both vertical and inclined imposed fields are considered. In this regime the leading order nonlinearity is provided by the distortion of the horizontally averaged temperature profile. For overstable convection this profile is determined from the solution of a nonlinear eigenvalue problem for the (time-averaged) Nusselt number and oscillation frequency, and evolves towards an isothermal profile with increasing Rayleigh number. In the presence of variable magnetic Prandtl number  $\zeta(z)$  the profile is asymmetric with respect to midlevel, but nonetheless develops an isothermal core in the highly supercritical regime. A hysteretic transition between two distinct convection regimes is identified in the inclined case, and used to suggest an explanation for the sharp boundary between the sunspot umbra and penumbra. These results are obtained via an asymptotic expansion in inverse powers of the Chandrasekhar number, and generalize readily to a polytropic atmosphere.

## 1 Introduction

The study of convection in an imposed magnetic field is motivated primarily by astrophysical applications, particularly by the observed magnetic field dynamics in the solar convection zone (Hughes and Proctor 1988). Applications to sunspots (Thomas and Weiss 1992) have led several authors to investigate the suppression of convection by strong magnetic fields. The linear and weakly nonlinear theory describing this suppression is summarized by Chandrasekhar (1961) and Proctor and Weiss (1982).

In this paper we summarize a recent development that allows us to extend these strong-field results, semi-analytically, into the fully nonlinear regime and generalize it to include background stratification. The resulting solutions are valid at Rayleigh numbers arbitrarily far above onset. These solutions are constructed via an asymptotic expansion in inverse powers of the Chandrasekhar number  $Q$ .

This dimensionless number measures the strength of the imposed magnetic field and in the large  $Q$  limit leads to a simplified set of dynamical equations. In these equations the dominant nonlinearity arises from the nonlinear distortion of the mean temperature profile; the strong magnetic field resists distortion by the velocity field and the Lorentz force arising from the distortion of the magnetic field remains small. As a result our solutions are characterized by a single wavenumber in the horizontal with the vertical structure given by the solution of a nonlinear eigenvalue problem for the Nusselt number. The derivation of this nonlinear eigenvalue problem can be performed analytically although the problem itself must be solved numerically, and can be performed for both steady and oscillatory magnetoconvection and for both vertical and tilted imposed fields. Although these results are formally obtained for stress-free boundary conditions, in the strong magnetic field limit they describe the dynamics outside of narrow boundary layers for other types of boundary conditions as well.

Of particular interest is the fact that our approach applies equally to the case in which the magnetic Prandtl number  $\zeta$  depends nontrivially on the depth  $z$  within the layer. Not only does this allow us to explore more realistic profiles of the magnetic and thermal diffusivities but it also makes accessible the interesting case in which  $\zeta$  passes through one somewhere in the layer. Recall that near the surface of the solar convection zone ( $1,500 \text{ km} < z < 20,000 \text{ km}$ ) the thermal diffusivity is reduced owing to the increase in opacity caused by ionization and in this region  $\zeta > 1$ , favouring steady convection. Both above and below this region  $\zeta < 1$ , favouring overstable convection. It has been suggested (Knobloch and Weiss 1984, Weiss *et al.* 1990) that these changes in  $\zeta$  are responsible for the presence of umbral dots with the more efficient steady convection penetrating into the overlying regions of less efficient overstable convection and forming the intermittent bright spots observed in sunspot umbrae. Our solutions in this regime lend further support to this idea. We find strongly nonlinear two- and three-dimensional solutions in which overturning convection in the lower part of the layer is coupled to overstable convection in the upper part. The resulting solution is periodic in time but the oscillation amplitude is small near the bottom and large near the top. Moreover the oscillation period becomes independent of the applied Rayleigh number at high Rayleigh numbers indicating that the oscillation is of magnetic origin. In the case of tilted magnetic field our methods permit us to construct two-dimensional solutions only. Although not as general, these solutions reveal an unexpected and important transition with increasing Rayleigh number to a novel form of convection in which the input heat is converted into magnetic energy instead of being transported across the layer. This transition occurs only for sufficiently large tilt angles and is hysteretic, and may be related to the abrupt transition from umbra to penumbra observed in sunspots. As a first step towards a realistic sunspot model based on these ideas we also describe how our methods generalize to a stratified atmosphere.

## 2 Formulation of the Problem

We begin with Boussinesq magnetoconvection in a plane horizontal layer described by the dimensionless equations

$$\frac{1}{\sigma} \frac{D\mathbf{v}}{Dt} = -\nabla\pi + \zeta Q \mathbf{B} \cdot \nabla \mathbf{B} + RaT \hat{\mathbf{z}} + \nabla^2 \mathbf{v}, \quad (1)$$

$$\frac{DT}{Dt} = \nabla^2 T, \quad (2)$$

$$\frac{D\mathbf{B}}{Dt} = \mathbf{B} \cdot \nabla \mathbf{v} - \nabla \times (\zeta \nabla \times \mathbf{B}), \quad (3)$$

$$\nabla \cdot \mathbf{v} = 0, \quad \nabla \cdot \mathbf{B} = 0. \quad (4)$$

Here  $\mathbf{v} = (u, v, w)$  is the velocity field in Cartesian coordinates  $(x, y, z)$  with  $z$  vertically upwards. The symbol  $T$  denotes the temperature, while  $\pi$  is the total (thermal and magnetic) pressure. The velocity field is written in the form  $\mathbf{v} = \bar{\mathbf{U}} + \mathbf{u}$ , where  $\bar{\mathbf{U}}(z)$  is a possible mean flow and  $\mathbf{u}(x, y, z, t)$  is the convective flow. Likewise, the dimensionless magnetic field is assumed to be the superposition  $\mathbf{B} = \hat{\mathbf{r}} + \bar{\mathbf{B}} + \mathbf{b}$  of an imposed oblique field of unit strength, a mean field  $\bar{\mathbf{B}}(z)$ , and a three-dimensional field  $\mathbf{b}(x, y, z, t)$  both due to the presence of convection. The oblique field is denoted by  $\hat{\mathbf{r}} = (\sin \vartheta, 0, \cos \vartheta)$ , where  $\vartheta$  denotes the angle with respect to the vertical in the  $(x, z)$  plane. The equations have been nondimensionalized with respect to the thermal diffusion time in the vertical. The resulting dimensionless parameters

$$Q = \frac{B_0^2 d^2}{\mu_0 \rho \eta \nu}, \quad Ra = \frac{g \alpha \Delta T d^3}{\nu \kappa}, \quad \sigma = \frac{\nu}{\kappa}, \quad \zeta = \frac{\eta}{\kappa}, \quad (5)$$

are the Chandrasekhar, Rayleigh, and thermal and magnetic Prandtl numbers, respectively. We write

$$\begin{aligned} \mathbf{u}(x, y, z, t) &= \nabla \times \phi(x, y, z, t) \hat{\mathbf{z}} + \nabla \times \nabla \times \psi(x, y, z, t) \hat{\mathbf{z}}, \\ \mathbf{b}(x, y, z, t) &= \nabla \times A(x, y, z, t) \hat{\mathbf{z}} + \nabla \times \nabla \times B(x, y, z, t) \hat{\mathbf{z}}. \end{aligned} \quad (6)$$

Equations (1-4) are solved for a fluid confined between boundaries at fixed temperatures,

$$T(0) = 1, \quad T(1) = 0, \quad (7)$$

which are impenetrable and either stress-free or no-slip at the top and bottom. The simplest magnetic boundary conditions, employed by Matthews *et al.* (1992), require that the field be tilted by the same angle  $\vartheta$  to the vertical everywhere on the top and bottom boundaries. However, in the large  $Q$  limit the detailed nature of the boundary conditions becomes unimportant: the solutions for different magnetic or velocity boundary conditions differ in thin boundary layers at top and bottom only. Periodic boundary conditions in the horizontal are assumed.

For large values of the Chandrasekhar number  $Q$  simplified equations describing the nonlinear problem can be obtained using the scaling (cf. Julien *et al.* 1999, 2000)

$$(x, y) = Q^{-\frac{1}{4}}(x', y'), \quad t = Q^{-\frac{1}{2}}t'. \quad (8)$$

With this scaling we focus on small horizontal scales (and high frequency oscillations in the case of overstable convection). For an alternative scaling see Matthews (1999). Because the strong magnetic field tends to align the cells with the tilt we expect the solutions to manifest small scale oscillations in the vertical with an  $\mathcal{O}(Q^{\frac{1}{4}})$  vertical wavenumber, in addition to variation on the usual  $\mathcal{O}(1)$  scale corresponding to the layer depth. We denote these scales by  $z'$  and  $Z$ , respectively, and write

$$\partial_x, \partial_y = Q^{\frac{1}{4}}(\partial_{x'}, \partial_{y'}), \quad \partial_z = Q^{\frac{1}{4}}\partial_{z'} + D, \quad \partial_t = Q^{\frac{1}{2}}\partial_{t'}, \quad (9)$$

where  $D \equiv \partial_Z$ . Throughout we focus on  $\mathcal{O}(Q)$  Rayleigh numbers, i.e., we also write  $Ra = QRa'$ . The Prandtl numbers  $\sigma$  and  $\zeta$  are not scaled and remain of order one. However, the latter is allowed to vary with depth. The resulting expansion reflects the tendency towards small scale motion aligned with the inclined magnetic field and describes correctly not only the linear and nonlinear properties of solutions with these wavenumbers but also those with the  $\mathcal{O}(Q^{\frac{1}{6}})$  wavenumbers selected by linear theory (Chandrasekhar 1961). In addition the analysis with  $\mathcal{O}(Q^{\frac{1}{4}})$  wavenumbers captures the transition from overstable convection preferred at small  $\zeta$  to steady overturning convection preferred for  $\zeta > 1$ . Next, we scale the fluid variables such that all three components of the velocity and magnetic field perturbations are comparable, with  $\mathbf{u} \approx \mathcal{O}(Q^{\frac{1}{4}})$  and  $\mathbf{b} \approx \mathcal{O}(Q^{-\frac{1}{4}})$ , i.e., we write

$$\phi = \phi'(x', y', z', Z, t'; Q), \quad (10)$$

$$\psi = Q^{-\frac{1}{4}}\psi'(x', y', z', Z, t'; Q), \quad (11)$$

$$A = Q^{-\frac{1}{2}}A'(x', y', z', Z, t'; Q), \quad (12)$$

$$B = Q^{-\frac{3}{4}}B'(x', y', z, Z, t'; Q). \quad (13)$$

Finally, to allow substantial deformation of the mean temperature gradient, we write

$$T = \theta_0(Z; Q) + Q^{-\frac{1}{4}}\theta'(x', y', z', Z, t'; Q), \quad (14)$$

where  $\theta'$  denotes the fluctuations from the mean. In the following we drop all primes.

The above scaling works for both stress-free and no-slip boundary conditions at top and bottom since it describes the dynamics in the bulk, i.e., outside of thin boundary layers required by specific velocity and magnetic field boundary conditions. (Julien *et al.* 1999, 2000). The resulting equations are solved by an asymptotic expansion in powers of  $Q^{-\frac{1}{4}}$  of the form

$$\Psi = \Psi_1 + Q^{-\frac{1}{4}}\Psi_2 + Q^{-\frac{1}{2}}\Psi_3 + \dots, \quad (15)$$

where  $\Psi \equiv (\phi, \psi, \theta, A, B)^T$ . At  $\mathcal{O}(Q^0)$  one obtains

$$\hat{\mathbf{r}} \cdot \nabla_0 \phi_1 = 0, \quad \hat{\mathbf{r}} \cdot \nabla_0 \psi_1 = 0, \quad \hat{\mathbf{r}} \cdot \nabla_0 A_1 = 0, \quad \hat{\mathbf{r}} \cdot \nabla_0 B_1 = 0. \quad (16)$$

Thus on small scales all perturbations align with the imposed magnetic field. Solutions of this type take the form

$$\Psi_1(\mathbf{x}, Z, t) = \int \Psi_1(\mathbf{k}_0, Z, t) e^{i\mathbf{k}_0 \cdot \mathbf{x}} d\mathbf{k}_0 + \text{c.c.}, \quad (17)$$

where  $\mathbf{k}_0 \cdot \hat{\mathbf{r}} = 0$ . Since  $\hat{\mathbf{r}} = (\sin \vartheta, 0, \cos \vartheta)$  and  $(k_{0x}, k_{0y}) = k_{0\perp}(\cos \chi, \sin \chi)$  it follows that  $k_{0z} = -k_{0x} \tan \vartheta = -k_{0\perp} \cos \chi \tan \vartheta$ . The solvability condition at  $\mathcal{O}(Q^{-\frac{1}{4}})$  yields evolution equations for the amplitudes  $\Psi_1(\mathbf{k}_0, Z, t)$ :

$$\frac{1}{\sigma} \left( \partial_t \phi_1 - \frac{1}{k_{0\perp}^2} P N_\phi(\Psi_1) \right) = \zeta \left( \hat{r}_z D A_1 - \frac{1}{k_{0\perp}^2} P M_\phi(\Psi_1) \right) - k_0^2 \phi_1, \quad (18)$$

$$\frac{1}{\sigma} \left( \partial_t \psi_1 + \frac{1}{k_0^2 k_{0\perp}^2} P N_\psi(\Psi_1) \right) = \frac{Ra}{k_0^2} \theta_1 + \zeta \left( \hat{r}_z D B_1 + \frac{1}{k_0^2 k_{0\perp}^2} P M_\psi(\Psi_1) \right) - k_0^2 \psi_1, \quad (19)$$

$$\partial_t A_1 - \frac{1}{k_{0\perp}^2} P M_A(\Psi_1) = \hat{r}_z D \phi_1 - \zeta k_0^2 A_1, \quad (20)$$

$$\partial_t B_1 - \frac{1}{k_{0\perp}^2} P M_B(\Psi_1) = \hat{r}_z D \psi_1 - \zeta k_0^2 B_1, \quad (21)$$

where  $P$  is a projection operator that filters out the fast spatial variation, defined by

$$P f(\Psi_1) \equiv \frac{1}{(2\pi)^3} \int e^{-i\mathbf{k}_0 \cdot \mathbf{x}} f(\Psi_1) d\mathbf{x}, \quad (22)$$

and the quantities  $M, N$  denote nonlinear terms. Explicit expressions for these terms can be found in Julien *et al.* (1999).

The temperature equation yields the following equations at  $\mathcal{O}(Q^{\frac{1}{4}})$  and  $\mathcal{O}(Q^0)$ , respectively,

$$\partial_t \theta_1 - J[\phi_1, \theta_1] + \left( \nabla_{0\perp} \partial_z \psi_1 \cdot \nabla_{0\perp} \theta_1 - \nabla_{0\perp}^2 \psi_1 \partial_z \theta_1 \right) - \nabla_{0\perp}^2 \psi_1 D \theta_0 = \nabla_0^2 \theta_1, \quad (23)$$

$$\begin{aligned} & \partial_t \theta_2 - J[\phi_1, \theta_2] - J[\phi_2, \theta_1] + \left( \nabla_{0\perp} \partial_z \psi_1 \cdot \nabla_{0\perp} \theta_2 - \nabla_{0\perp}^2 \psi_1 \partial_z \theta_2 \right) \quad (24) \\ & + \left( \nabla_{0\perp} \partial_z \psi_2 \cdot \nabla_{0\perp} \theta_1 - \nabla_{0\perp}^2 \psi_2 \partial_z \theta_1 \right) + \left( \nabla_{0\perp} D \psi_1 \cdot \nabla_{0\perp} \theta_1 - \nabla_{0\perp}^2 \psi_1 D \theta_1 \right) \\ & - \nabla_{0\perp}^2 \psi_2 D \theta_0 = \nabla_0^2 \theta_2 + 2\partial_z D \theta_1 + D^2 \theta_0. \end{aligned}$$

Here the symbol  $J(f, g)$  denotes the horizontal Jacobian  $f_x g_y - f_y g_x$ . Equation (23) can be solved for  $\theta_1$ . Once this is done the solvability condition for the mean part of  $\theta_2$  yields

$$D^2 \theta_0 + D(\overline{\nabla_{0\perp}^2 \psi_1 \theta_1}) = 0, \quad (25)$$

which can be integrated once, obtaining

$$D\theta_0 + \overline{\nabla_{\perp}^2 \psi_1} \theta_1 = -K. \quad (26)$$

For steady patterns the constant  $K$  is identified with the Nusselt number; for oscillatory patterns we extend the meaning of the overbar to indicate an average over time as well. For such patterns  $K$  represents the time-averaged Nusselt number.

Equations (18-21) and (23,26) constitute a closed set of equations for the vertical profiles of the different fields. The simplest case of such evolution is offered by (tilted) two-dimensional solutions of the form

$$\Psi_1 = \Psi_L(Z) \exp(i\omega t + i\mathbf{k}_0 \cdot \mathbf{x}) + \Psi_R(Z) \exp(i\omega t - i\mathbf{k}_0 \cdot \mathbf{x}) + \text{c.c.} \quad (27)$$

For these solutions the nonlinear terms in equations (18-21) vanish and consequently the toroidal fields  $\phi_1$ ,  $A_1$  also vanish (Julien *et al.* 1999). The remaining quantities  $\psi_1$ ,  $B_1$  and  $\theta_1$  satisfy *linear* equations:

$$\left(\frac{i\omega}{\sigma} + k_0^2\right) k_0^2 \psi_{(L,R)} = Ra\theta_{(L,R)} + \zeta k_0^2 \hat{r}_z DB_{(L,R)} \quad (28)$$

$$(i\omega + \zeta k_0^2) B_{(L,R)} = \hat{r}_z D\psi_{(L,R)}, \quad (29)$$

$$(i\omega + k_0^2) \theta_{(L,R)} = -k_{0\perp}^2 \psi_{(L,R)} D\theta_0. \quad (30)$$

These coupled equations may be collapsed using the transformation

$$\Psi_{1L} = \frac{\Psi_1}{\sqrt{1+|c|^2}}, \quad \Psi_{1R} = \frac{c \Psi_1}{\sqrt{1+|c|^2}}, \quad (31)$$

where  $c = 0(1)$  for travelling (standing) waves. Here  $\Psi_1(Z) = (\Psi(Z), B(Z), \Theta(Z))$ . From equation (26) we now obtain

$$D\theta_0 \left[ 1 + \frac{2k_0^2 k_{0\perp}^4}{\omega^2 + k_0^4} |\Psi|^2 \right] = -K, \quad (32)$$

with  $K$  given by the requirement that  $\theta_0(0) = 1$ ,  $\theta_0(1) = 0$ :

$$K = \left[ \int_0^1 \frac{\omega^2 + k_0^4}{\omega^2 + k_0^4 + 2k_0^2 k_{0\perp}^4 |\Psi|^2} dZ \right]^{-1}, \quad (33)$$

while equations (28-30) yield the nonlinear eigenvalue problem

$$D^2 \Psi - \frac{(D\zeta) k_0^2}{i\omega + \zeta k_0^2} D\Psi - \frac{1}{\hat{r}_z^2 \zeta} \left( \frac{i\omega}{\sigma} + k_0^2 \right) (i\omega + \zeta k_0^2) \Psi + \frac{RaK}{\hat{r}_z^2 \zeta} \frac{(i\omega + \zeta k_0^2)(-i\omega + k_0^2) k_{0\perp}^2}{\omega^2 + k_0^4 + 2k_0^2 k_{0\perp}^4 |\Psi|^2} \frac{k_0^2}{k_0^2} \Psi = 0. \quad (34)$$

The solutions of this problem depend on the prescribed function  $\zeta(z)$  as well as the parameters  $Ra$ ,  $k_0$ ,  $k_{0\perp}$  and  $\sigma$ . The corresponding results for a vertical magnetic field are recovered on setting  $\hat{r}_z = 1$  (Julien *et al.* 1999). Note that steady solutions ( $\omega = 0$ ) are independent of both  $\sigma$  and  $\zeta$ , at least if  $\zeta$  is depth-independent. The latter is not generally true and for finite  $Q$  the steady solutions do depend on  $\zeta$ .

## 2.1 Dynamics and symmetry

The solutions obtained by solving the nonlinear eigenvalue problem (34) represent a special type of simple, stationary, spatially periodic solutions. Despite their simplicity these solutions are important. For example, Julien *et al.* (1999) show that in the case of an imposed vertical field all spatially periodic three-dimensional solutions possess the same (time-averaged) Nusselt number and frequency. The selection among these planforms is due to subdominant eigenvalues describing their relative stability but absent from the theory. In addition to this lack of planform selection there is one other effect that disappears in the large  $Q$  limit. Boussinesq convection in a tilted field has a special property: the equations (and boundary conditions) are equivariant (i.e., symmetric) under a reflection in a vertical plane followed by a reflection in the midplane of the layer. As a result if a left-travelling wave is a solution so is a right-travelling wave, and consequently so are standing waves. Moreover, steady solutions in the form of tilted convection cells are also possible. However, as noted by Matthews *et al.* (1992) and discussed in more detail by Knobloch (1994), when the properties of the layer depend on depth the midplane symmetry is usually lost. In this case there are generically no steady state bifurcations from the conduction state and the primary instability is a Hopf bifurcation to travelling waves with a *preferred* direction of propagation selected by the tilt together with the depth-dependence. There are also no bifurcations to standing waves, the counterparts of which are quasiperiodic waves that appear in a secondary bifurcation from the primary travelling wave branch. These effects are absent in our limit because they rely on frequency splitting due to the depth-dependence and this remains of order one, i.e., on the  $\mathcal{O}(Q^{\frac{1}{2}})$  timescale the drift of our steady solutions is negligible and so is the second frequency accompanying our standing waves, or the frequency difference between left- and right-travelling waves. Likewise, the splitting in the critical Rayleigh numbers for the onset of left- and right-travelling waves remains  $\mathcal{O}(1)$  and hence small compared to the  $\mathcal{O}(Q)$  Rayleigh numbers considered. It is important to bear these facts in mind when interpreting the solutions described below.

These shortcomings notwithstanding, the asymptotic equations (18-23,26) provide a much simplified description of the *dynamics* of the system in the high  $Q$  limit. The resulting equations for three-dimensional magnetoconvection in a vertical field,

$$\frac{1}{\sigma}\partial_t\phi_1 = \zeta(z)DA_1 + \nabla_{\perp}^2\phi_1, \quad (35)$$

$$\frac{1}{\sigma}\partial_t\nabla_{\perp}^2\psi_1 = -Ra\theta_1 + \zeta(z)D\nabla_{\perp}^2B_1 + \nabla_{\perp}^4\psi_1, \quad (36)$$

$$\partial_tA_1 = D\phi_1 + \zeta(z)\nabla_{\perp}^2A_1, \quad (37)$$

$$\partial_tB_1 = D\psi_1 + \zeta(z)\nabla_{\perp}^2B_1, \quad (38)$$

$$\partial_t\theta_1 - \nabla_{\perp}^2\theta_1 = \nabla_{\perp}^2\psi_1 D\theta_0, \quad (39)$$

coupled via (26), bear a considerable similarity to those derived Babin *et al.* (1994) for rapidly rotating turbulence. These equations have an invariant subspace  $\phi_1 = A_1 = 0$ . The dynamics in this subspace are described by equations (36,38,39) and (26); at finite amplitude vortical motion may be excited by secondary instabilities, resulting in the spontaneous generation of helicity, both fluid and magnetic. However, even aside from this interesting possibility, it is clear that the dynamics in the zero-helicity invariant subspace can be turbulent, much as in the related problem of rapidly rotating convection (Julien *et al.* 1998), i.e., that the solutions described by the nonlinear eigenvalue problem (34) need not be stable, particularly if three-dimensional periodic boxes with spatial period larger than  $2\pi/k_{0\perp}$  are employed. Simulations of these equations (and of equations (18-23,26)) in these circumstances are therefore of fundamental interest and will be described elsewhere.

### 3 Results

In this section we summarize the results obtained thus far from the nonlinear eigenvalue problem (34). This problem is to be solved subject to the boundary conditions

$$\Psi(0) = \Psi(1) = 0, \quad (40)$$

imposing impermeability of the boundaries. Once this is done the mean (i.e., averaged horizontally and in time) temperature profile  $\theta_0$  can be found from the relation (32). The calculations are performed on a discretised one-dimensional mesh using an iterative Newton-Raphson-Kantorovich scheme with  $\mathcal{O}(10^{-10})$  accuracy in the  $L_2$  norm of  $\Psi(Z)$  and the corresponding eigenvalues. For each  $Ra$  the solution determines  $K$  and  $\omega$  as eigenvalues of equation (34) and the associated eigenfunction  $\Psi(Z)$ .

In the following we present results first for the case of a vertical magnetic field ( $\vartheta = 0$ ), and then discuss the case of an inclined field ( $\vartheta \neq 0$ ) in the two cases  $\chi = 0$ ,  $\chi = \pi/2$  (see fig. 1). All results are obtained with the horizontal wavenumber  $k_{0\perp} = 1$  and Prandtl number  $\sigma = 1.1$ . (In Julien *et al.* (1999) solutions are obtained for both  $k_{0\perp} = 1$  and  $k_0 = 1$ .)

#### 3.1 Linear theory

We first summarize the linear stability properties of the conduction solution  $\mathbf{v} = 0$ ,  $T = 1 - z$ ,  $\mathbf{B} = \hat{\mathbf{r}}$  in the two cases  $\chi = 0$ ,  $\chi = \pi/2$  obtained from the full equations with stress-free boundaries and fixed field inclination. Fig. 2 shows the critical Rayleigh number  $Ra_c$  and the corresponding wavenumber  $k_c$  as a function of  $Q$  for steady and oscillatory convection for several different values of the tilt angle  $\vartheta$  when  $\chi = 0$ . As expected, when  $\chi = 0$  the critical Rayleigh number increases rapidly with increasing  $Q$ , i.e., the inclined magnetic field has a stabilizing effect. This effect depends only weakly on the tilt angle but decreases as this angle increases.

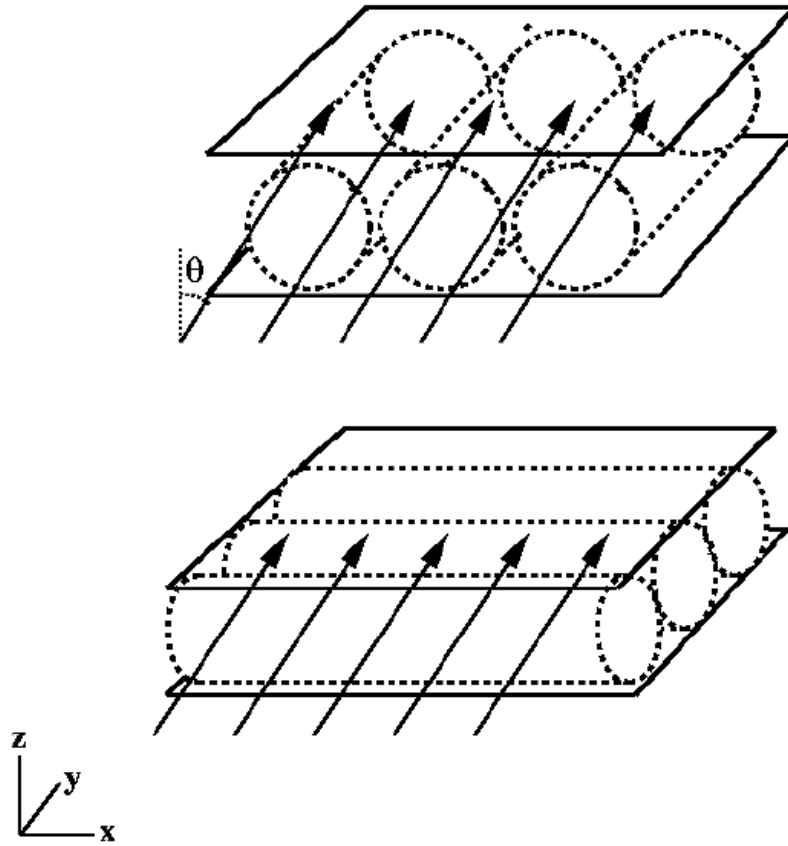


Figure 1: A sketch indicating the orientation of perpendicular ( $\chi = 0$ ) and parallel ( $\chi = \pi/2$ ) rolls.

Fig. 2c shows the approach of  $Ra_c(Q)$  to its asymptotic behaviour, and confirms that in this regime  $Ra_c = \mathcal{O}(Q)$  for the tilt angles considered. However, for large  $Q$  one expects  $k_c = \mathcal{O}(Q^{\frac{1}{6}})$  but this behaviour is found only for tilt angles that are small enough; for tilt angles exceeding approximately  $30^\circ$  an  $\mathcal{O}(1)$  wavenumber is selected instead. These results reflect the dominant component of the field: for steady convection in an imposed vertical field,  $k_c \sim (\frac{1}{2}\pi^4 Q)^{\frac{1}{6}}$  while for an imposed horizontal field,  $k_c \sim \pi^{\frac{3}{2}} Q^{-\frac{1}{4}}$ . In both cases  $Ra_c \sim \pi^2 Q$ . These two types of behaviour indicate that as the tilt angle increases the system undergoes a transition in which its behaviour changes from one in which the vertical field dominates to one in which the horizontal field dominates. We shall see that such a transition occurs in the nonlinear regime as well. In contrast, when  $\chi = \pi/2$   $k_c \sim (\frac{1}{2}\pi^4 Q \cos^2 \vartheta)^{\frac{1}{6}}$ ,  $Ra_c \sim \pi^2 \cos^2 \vartheta Q$ , provided that  $Q \cos^2 \vartheta \gg 1$ , and the transition to the horizontal field behaviour occurs only for tilt angles  $\vartheta = \pi/2 - \mathcal{O}(Q^{-\frac{1}{2}})$ , i.e., for horizontal fields. In this case the magnetic field has no effect on the onset of convection and the selected wavenumber is therefore  $\mathcal{O}(1)$ . Thus in either case large wavenumbers are selected for tilt angles that are not too large.

These results are to be compared with those obtained from the linearized eigenvalue problem (34). For constant  $\zeta$  we obtain

$$Ra^{(s)} = (1 + \cos^2 \chi \tan^2 \vartheta) \left[ \pi^2 \cos^2 \vartheta + (1 + \cos^2 \chi \tan^2 \vartheta)^2 k_{0\perp}^4 \right] Q, \quad (41)$$

where  $k_0^2 = k_{0\perp}^2 (1 + \cos^2 \chi \tan^2 \vartheta)$ . The minimum occurs at  $k_{0\perp} = 0$ :

$$Ra_c^{(s)} = (1 + \cos^2 \chi \tan^2 \vartheta) \pi^2 \cos^2 \vartheta Q. \quad (42)$$

This equation predicts that for  $\chi = 0$   $Ra_c$  is independent of  $\vartheta$ , in good agreement with the results of fig. 2. Likewise, for  $\zeta < 1$ , the onset of overstable oscillations occurs at

$$Ra^{(o)} = (1 + \cos^2 \chi \tan^2 \vartheta) \left[ \frac{\sigma + \zeta}{\sigma(1 + \sigma)} \right] \left[ \pi^2 \cos^2 \vartheta \sigma \zeta + (1 + \sigma)(1 + \zeta)(1 + \cos^2 \chi \tan^2 \vartheta)^2 k_{0\perp}^4 \right] Q, \quad (43)$$

$$\omega^{(o)2} = \frac{\zeta}{(1 + \sigma)} \left[ (1 - \zeta) \pi^2 \cos^2 \vartheta \sigma - \zeta(1 + \sigma)(1 + \cos^2 \chi \tan^2 \vartheta)^2 k_{0\perp}^4 \right] Q. \quad (44)$$

Again, the minimum occurs at  $k_{0\perp} = 0$ :

$$Ra_c^{(o)} = (1 + \cos^2 \chi \tan^2 \vartheta) \left( \frac{\sigma + \zeta}{1 + \sigma} \right) \pi^2 \cos^2 \vartheta \zeta Q, \quad \omega_c^{(o)2} = \left( \frac{1 - \zeta}{1 + \sigma} \right) \pi^2 \cos^2 \vartheta \sigma \zeta Q \quad (45)$$

and is independent of  $\vartheta$  when  $\chi = 0$ . In these expressions the wavenumber  $k_{0\perp}$  is the *scaled* horizontal wavenumber. The selection of  $k_{0\perp} = 0$  is thus a reflection of the selection (in the exact problem) of a smaller wavenumber, viz.  $k_{0\perp} = \mathcal{O}(Q^{\frac{1}{6}})$  in unscaled variables. However, the  $Q^{\frac{1}{4}}$  scaling determines correctly the resulting minimum Rayleigh numbers and frequency. Moreover, as pointed out by

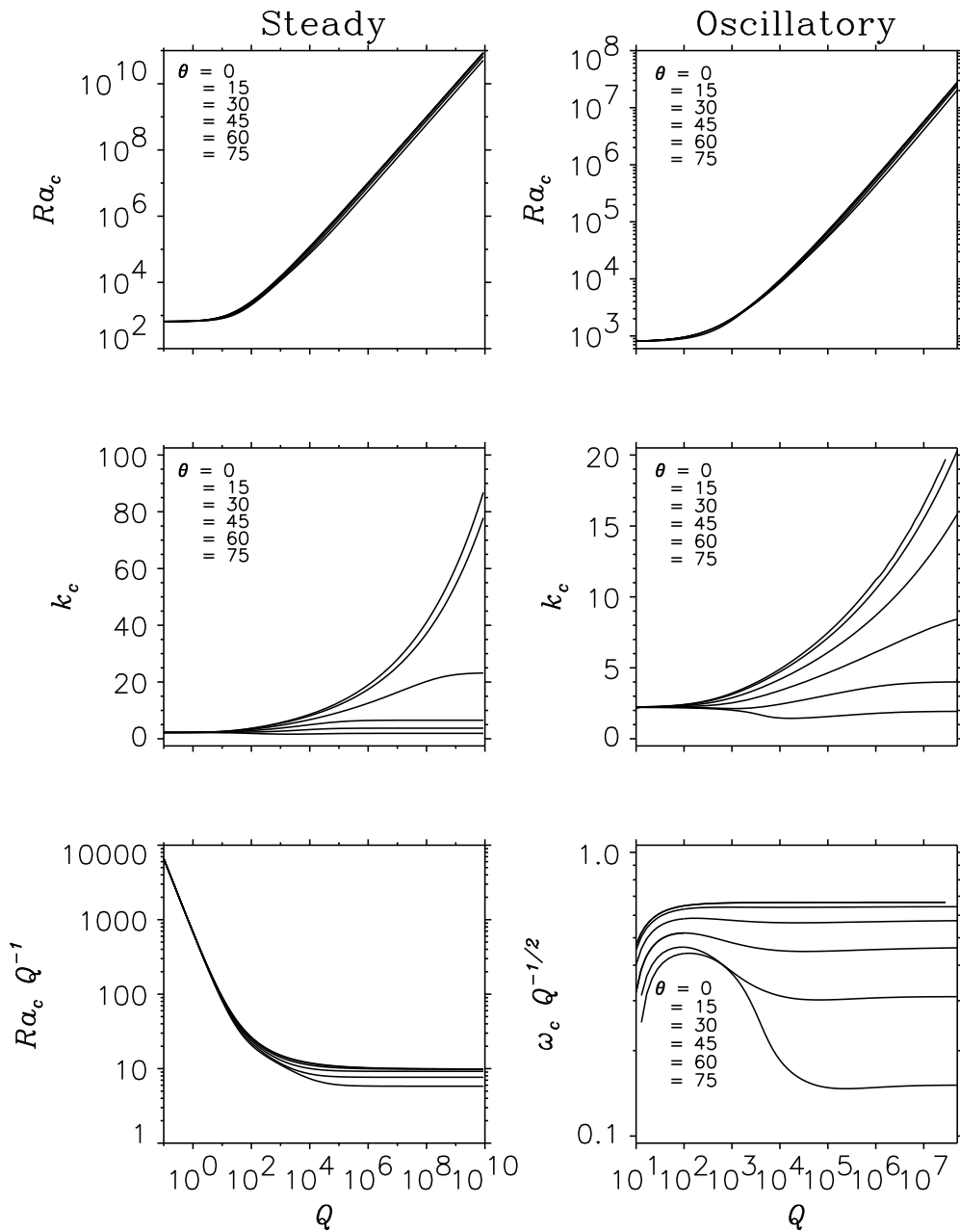


Figure 2: The critical Rayleigh number  $Ra_c$  and wavenumber  $k_c$  for onset of (i) steady, (ii) oscillatory perpendicular rolls ( $\chi = 0$ ) as functions of  $Q$  for several values of  $\vartheta$  and  $\zeta = 0.1$ . Figs. (c) show the approach of  $Ra_c(Q)$  to its asymptotic behaviour at large  $Q$ .

Chandrasekhar (1961), the  $\mathcal{O}(Q^{\frac{1}{4}})$  wavenumber scaling also captures the transition from steady to oscillatory convection. This transition takes place when  $\omega_c^{(o)} = 0$ , i.e., at

$$Ra_{TB} = (1 + \cos^2 \chi \tan^2 \vartheta) \left[ \frac{\sigma + \zeta}{\zeta(1 + \sigma)} \right] \pi^2 \cos^2 \vartheta Q, \quad (46)$$

$$k_{\perp TB} = \left[ \frac{\pi \cos \vartheta}{(1 + \cos^2 \chi \tan^2 \vartheta)} \right]^{\frac{1}{2}} \left[ \frac{\sigma(1 - \zeta)}{\zeta(1 + \sigma)} \right]^{\frac{1}{4}} Q^{\frac{1}{4}}, \quad (47)$$

and defines the Takens-Bogdanov (TB) point. Consequently the  $\mathcal{O}(Q^{\frac{1}{4}})$  scaling describes correctly not only the vicinity of the Takens-Bogdanov point but also the behaviour for onset wavenumbers far from this point, i.e., it allows us to retain the full wavenumber dependence of the problem.

For future reference we note that when  $\vartheta = 0$  all  $\chi$  dependence necessarily drops out. However, in contrast to the moderate  $Q$  results of Matthews *et al.* (1992)  $Ra_c(\chi = \pi/2) < Ra_c(\chi = 0)$  for all  $\vartheta \neq 0$  and hence away from the Takens-Bogdanov point parallel rolls are always selected at onset.

### 3.2 Vertical field with constant $\zeta$

In fig. 3 we show the (time-averaged) Nusselt number  $K$  and frequency for both steady and overstable convection in a vertical field as a function of the scaled Rayleigh number  $Ra$ . Observe that solutions can be obtained for highly supercritical Rayleigh numbers and that  $K$  increases monotonically with increasing  $Ra$  while the frequency  $\omega$  appears to saturate, indicating that the oscillations are of magnetic origin. Figs. 4 and 5 show the corresponding mean temperature profiles  $\theta_0 \equiv \bar{T}(z)$  for several values of  $Ra$ . For both steady and oscillatory convection the temperature gradients are confined to thinner and thinner boundary layers at the top and bottom as  $Ra$  increases. At the same time the bulk of the layer becomes more and more isothermal. Note that these boundary layers are symmetrical with respect to  $z = 1/2$  and that the isothermal interior has temperature  $T = 1/2$ , i.e., a temperature that is exactly half way between the temperatures at the top and bottom boundaries.

### 3.3 Vertical field with depth-dependent $\zeta$

The situation changes dramatically when  $\zeta \equiv \zeta(Z)$ . We follow Weiss *et al.* (1990,1996) and Julien *et al.* (1999, 2000) and choose a linear dependence on depth,  $\zeta(Z) = \zeta_0 + \epsilon(1 - Z)$ , focusing on the case in which  $\zeta$  changes from favouring oscillatory convection at the top of the layer ( $\zeta < 1$ ) to favouring steady convection at the bottom of the layer ( $\zeta > 1$ ).

Fig. 6a shows the Nusselt number  $K(Ra)$  for several values of  $\epsilon$  when  $\zeta_0 = 1$ . Fig. 6b shows the corresponding results for the more interesting case  $\zeta_0 = 0.2$ . In this case the convective instability is oscillatory and consequently we also

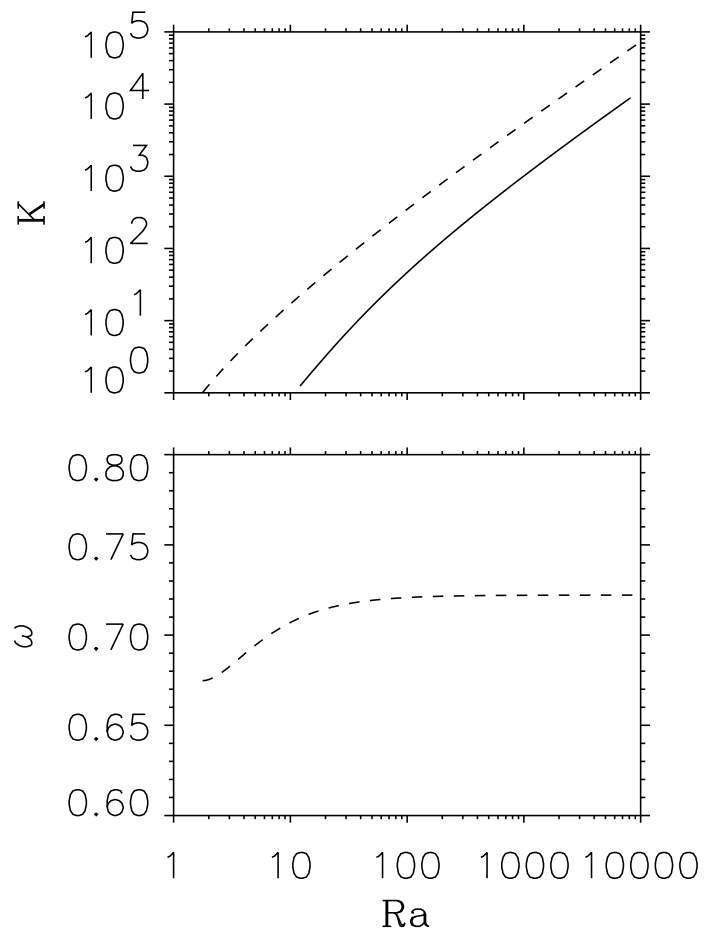


Figure 3: The (time-averaged) Nusselt number  $K$  for (a) steady (solid line) and oscillatory (dashed line) convection in a vertical field as a function of the scaled Rayleigh number  $Ra$  when  $\zeta = 0.1$  and  $\sigma = 1.1$ . Fig. (b) shows the corresponding (scaled) oscillation frequency  $\omega$ .

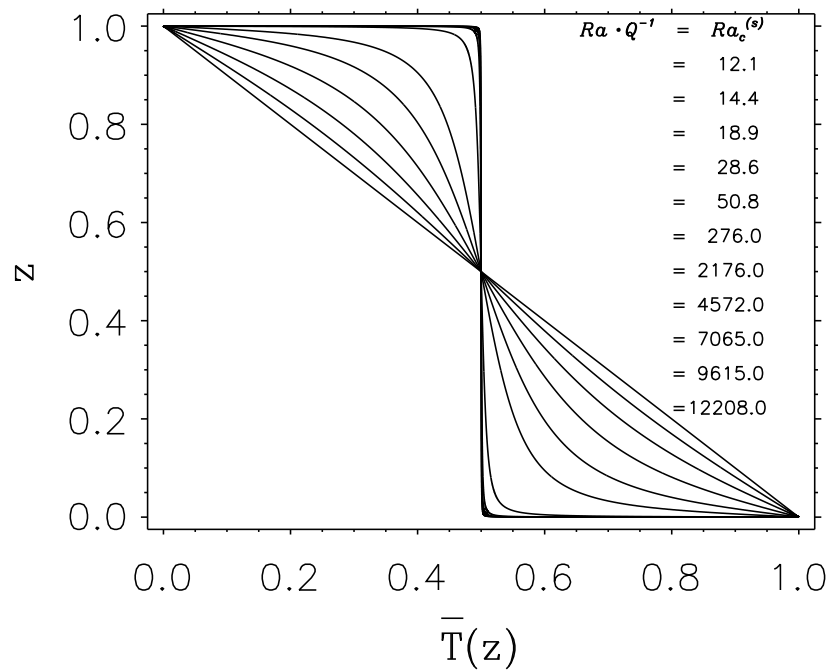


Figure 4: Mean temperature profiles  $\bar{T}(z)$  for steady convection at several values of the (scaled) Rayleigh number showing the development of an isothermal core with increasing  $Ra$  when  $\zeta = 0.1$

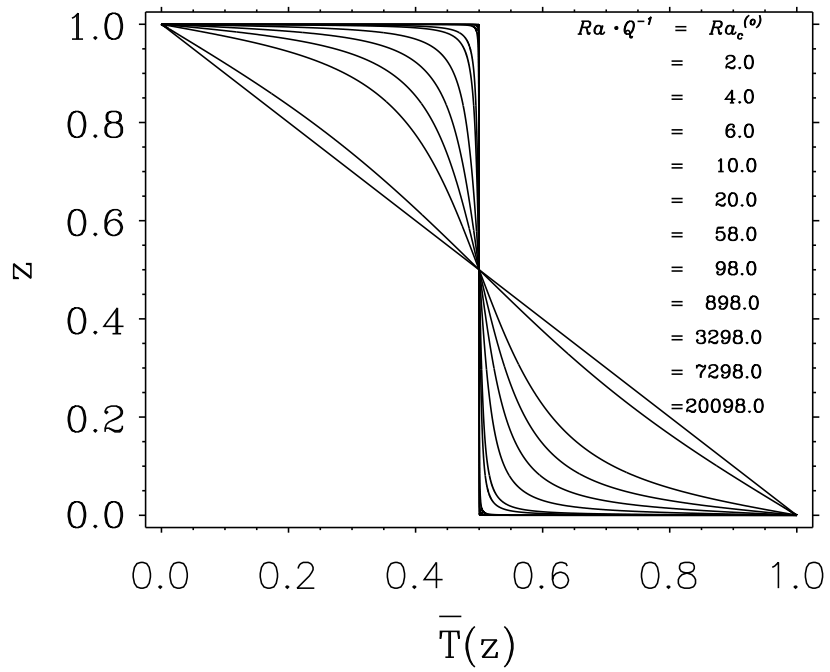


Figure 5: Same as fig. 4 but for oscillatory convection when  $\zeta = 0.1$ ,  $\sigma = 1.1$ .

show the oscillation frequency  $\omega$  (fig. 6c). These figures show that the differences between the effects of variable  $\zeta$  on steady and oscillatory convection extend into the nonlinear regime. In the steady case (fig. 6a) the Nusselt number is quite insensitive to  $\epsilon$  and one has to go to  $Ra$  values in excess of  $10^5$  to see a real difference. Nonetheless the trend is clear: at each Rayleigh number the Nusselt number decreases monotonically with increasing  $\epsilon$ . For oscillatory convection the  $\epsilon$  dependence is much stronger. As expected the Nusselt number is largest for small  $\epsilon$ . These solutions also have the smallest asymptotic frequency at large  $Ra$ ; not surprisingly this makes convective transport more efficient and hence increases the Nusselt number. In fig. 7 we show the dependence of the mean temperature profile on  $\epsilon$  at a high Rayleigh number in each of these two cases. Observe that as  $\epsilon$  increases away from zero the mean temperature profile acquires asymmetry with respect to the midplane  $z = 1/2$ . For large Rayleigh numbers the layer still develops an isothermal core but now its temperature  $T_{\text{core}}$  differs from  $T = 1/2$ . For steady convection with  $\epsilon > 0$   $T_{\text{core}} > 1/2$  while the opposite is the case when  $\epsilon < 0$ . Consequently the temperature jump in the upper boundary layer is larger than that in the lower one when  $\epsilon > 0$  and conversely. Once again the local decrease in the thermal diffusivity near the lower boundary makes convection easier near the bottom and hence we expect its maximum amplitude to fall below  $z = 1/2$  as  $\epsilon$  increases. In addition lower thermal diffusivity implies that at a given Rayleigh number the temperature jump across the lower thermal boundary layer also falls below  $1/2$ , as seen in fig. 7a. This is ultimately why  $T_{\text{core}}$  increases with  $\epsilon$ . Despite this appealing picture for steady convection the results for oscillatory convection reveal an opposite trend. Thus, as shown in fig. 7b, the core temperature moves towards lower values with increasing  $\epsilon$ , indicating that despite the decrease in thermal diffusivity near the bottom boundary the time-averaged temperature drop across the lower boundary layer increases. This is presumably because the repeated flow reversals do, on average, increase the boundary layer thickness, but what is unexpected is the magnitude of the resulting shift in the core temperature. Fig. 8 summarizes the shifts with  $\epsilon$  in the core temperatures in the two cases. Fig. 9 shows the profiles of the square of the eigenfunction  $|\psi_1(z)|$  in the oscillatory regime when  $\epsilon = 0.0$  and  $\epsilon = 1.0$ , both at onset and at  $Ra = 20106$ . When  $\epsilon = 0.0$  the profiles are symmetric, with largest amplitude at  $z = 1/2$ . When  $\epsilon > 0$  both profiles become asymmetric and peak above midheight; the effect is enhanced by nonlinearity.

As shown in fig. 10 nonlinear oscillations may be present even when linear theory predicts steady onset. In this case the oscillation frequency decreases to zero at finite amplitude where the branch of oscillatory solutions bifurcates from the steady branch (cf. Julien *et al.* 1999).

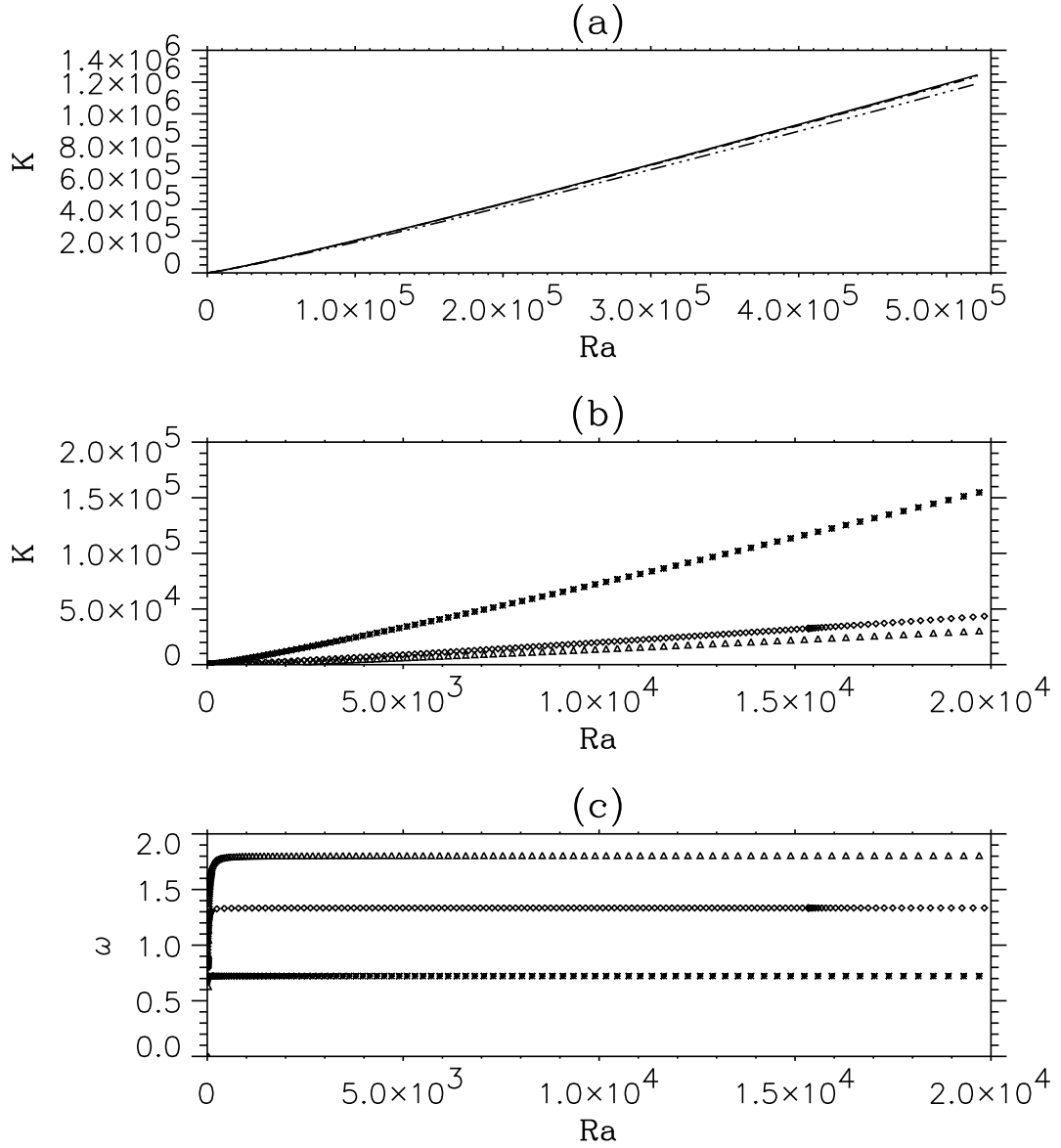


Figure 6: The Nusselt number  $K(Ra)$  for  $\zeta(Z) = \zeta_0 + \epsilon(1 - Z)$  at several values of  $\epsilon$  when  $\sigma = 1.1$ . (a) Steady convection when  $\zeta_0 = 1.0$  and  $\epsilon = 0.0$  (solid),  $\epsilon = 0.5$  (dashed),  $\epsilon = 1.0$  (dot-dashed) and  $\epsilon = 5.0$  (dot-dot-dot-dashed). (b) Oscillatory convection when  $\zeta_0 = 0.2$  and  $\epsilon = 0.0$  (asterisks),  $\epsilon = 2.0$  (diamonds) and  $\epsilon = 5.0$  (triangles). Fig. (c) shows the oscillation frequency  $\omega$  corresponding to (b). Notice that for steady convection  $K(Ra)$  remains largely independent of  $\epsilon$ , but for oscillatory convection both  $K$  and the asymptotic frequency  $\omega_\infty$  depend strongly on  $\epsilon$ .

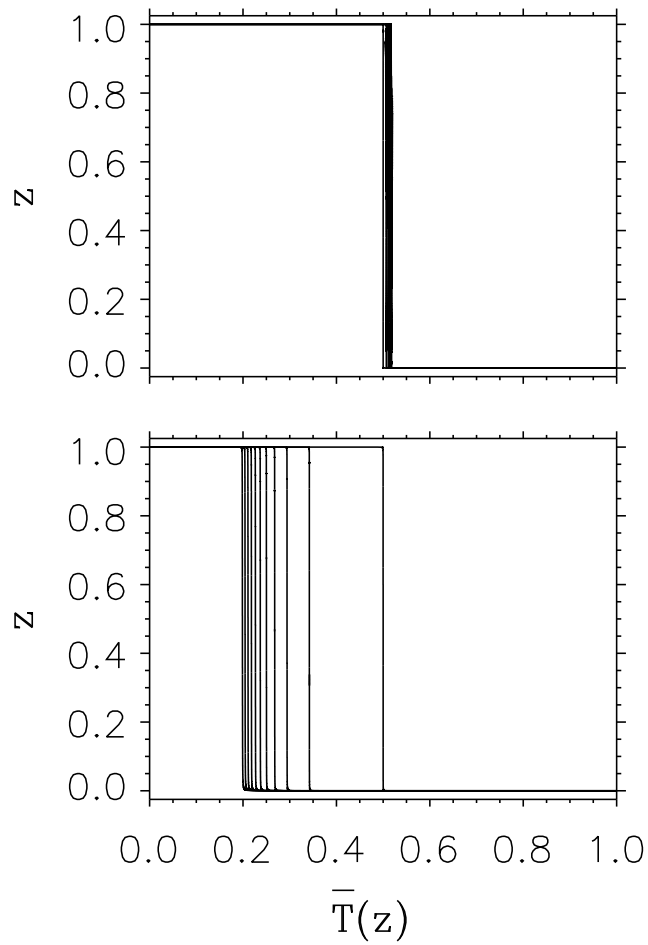


Figure 7: Mean temperature profiles  $\bar{T}(Z)$  for (a) steady convection and  $\epsilon = 0(1)5$  at  $Ra = 52100$  and (b) oscillatory convection as a function of  $\epsilon = 0(0.5)5$  at  $Ra = 20106$ ,  $\sigma = 1.1$ . The core temperature shifts monotonically from  $T_{\text{core}} = 1/2$  as  $\epsilon$  increases.

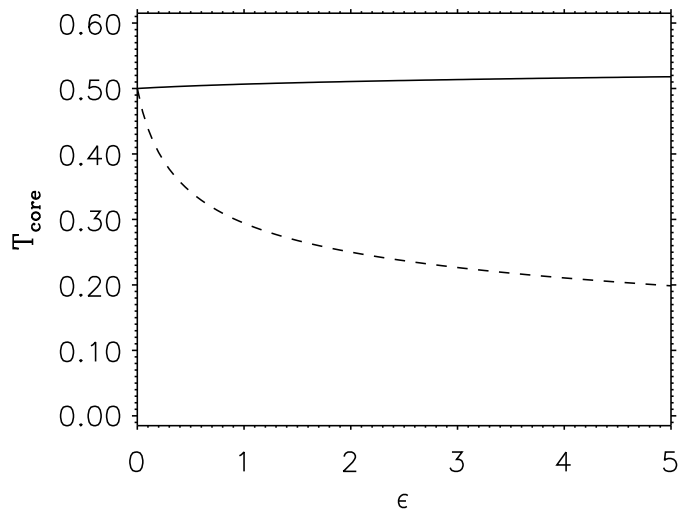


Figure 8: The core temperature  $T_{\text{core}}$ , determined from high Rayleigh number computations, as a function of  $\epsilon$  for steady convection (solid line) when  $\zeta_0 = 1.0$  and oscillatory convection (dashed line) when  $\zeta_0 = 0.2$ ,  $\sigma = 1.1$ . The isothermal core temperature increases slightly with increasing  $\epsilon$  in the steady case but decreases in the oscillatory case.

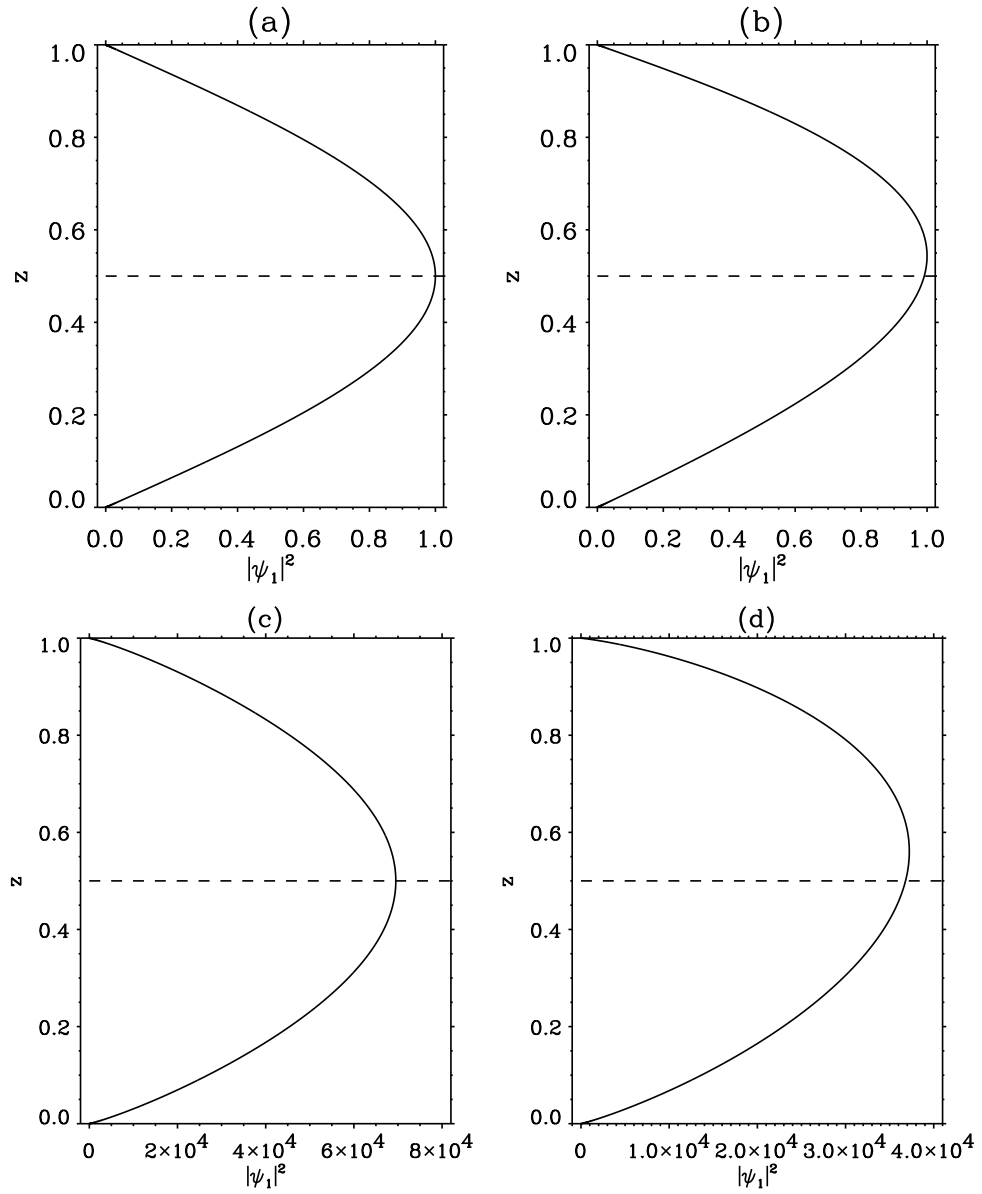


Figure 9: The square of the eigenfunction  $|\psi_1(Z)|$  for oscillatory convection at onset for (a)  $\epsilon = 0.0$  and (b)  $\epsilon = 1.0$ , showing the gradual development of localized oscillations in the upper part of the layer. (c,d) The corresponding  $|\psi_1(Z)|^2$  at  $Ra = 20106$ . The Prandtl number  $\sigma = 1.1$ .

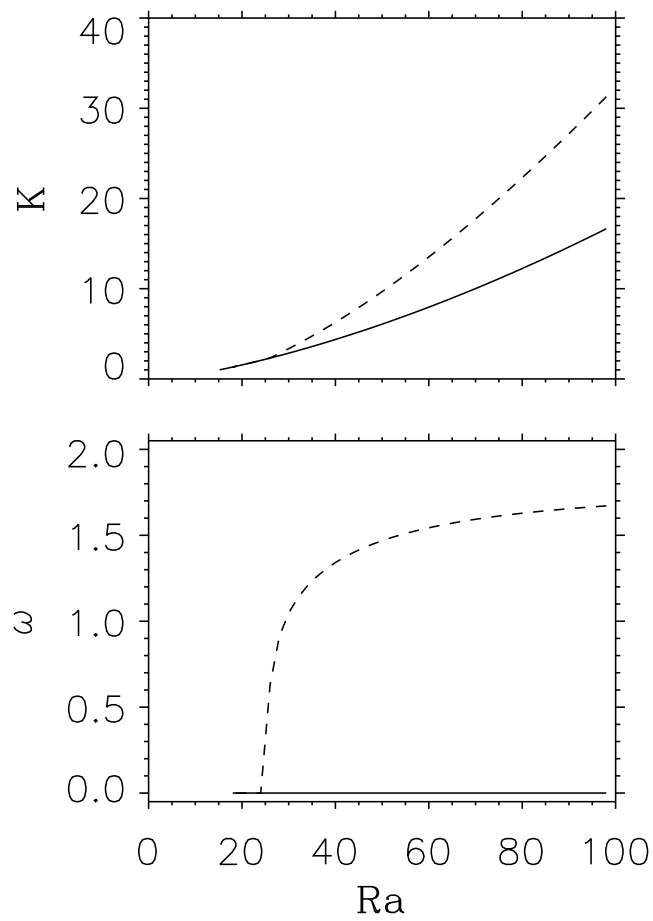


Figure 10: (a) The time-averaged Nusselt number  $K$  and (b) oscillation frequency  $\omega$  as functions of  $Ra$  for  $\epsilon = 5.0$ ,  $\sigma = 1.1$ .

### 3.4 Tilted field with constant $\zeta$

Calculations show that these results are not changed qualitatively when the magnetic field is tilted, provided that the tilt angle  $\vartheta$  is not too large. However, with increasing tilt both steady and oscillatory convection become less efficient at transporting heat, and the Rayleigh number dependence of the Nusselt number becomes weaker (see fig. 11). The increase in tilt angle leads to a larger Lorentz force, which in turn leads to a suppression of the heat transport. For the steady case the dependence on tilt angle is much weaker. This is to be expected since in the oscillatory regime ohmic diffusion has only a finite time to reduce the Lorentz force due to field distortion before the flow reverses and the Lorentz force depends strongly on the tilt angle. In contrast in the steady case the Lorentz force exerts a much weaker effect and the reduction of the Nusselt number is largely due to a geometrical effect: the strong oblique magnetic field inclines the convection cells relative to the vertical allowing them more time to lose their upward buoyancy to adjacent descending fluid.

Fig. 12 shows the corresponding results for the oscillatory mode when  $\vartheta = \pi/4$ . The figure reveals a remarkable behaviour: the Nusselt number  $K$  initially increases rapidly with  $Ra$  as in the vertical magnetic field case, but then undergoes a hysteretic transition to a new state characterized by a small Nusselt number, and one that *decreases* slowly with increasing  $Ra$ . Since the conductive flux increases with  $Ra$  the *convective* flux in this regime must decrease even more rapidly. As this state is followed to larger Rayleigh numbers we see that the mean temperature becomes almost piecewise linear (fig. 13), with a limited isothermal core. The extent of this core quickly saturates, in contrast to the case of a vertical field for which the isothermal core grows continuously with  $Ra$  as the temperature gradients are compressed into ever thinner thermal boundary layers (as in fig. 5). Evidently, in this state increasing the heat input does not result in increased heat transport across the layer. Instead, as discussed further below, the added energy is all stored in the magnetic field perturbations (since the field strength is large this is achieved with small deformation of the field); moreover, the perturbation magnetic field suppresses the convective motion in the boundary layers near the top and bottom (see fig. 13a) thereby reducing the transport of heat across the layer. These conclusions are supported by detailed computations of energy fluxes (Julien *et al.* 2000) and are a consequence of the fact that the flow must always cross magnetic field lines. In this regime (i.e., on the branch where the Nusselt number remains low as  $Ra$  is increased) the system of perpendicular rolls therefore behaves much more like one with an imposed *horizontal* field.

Fig. 13b indicates that the new regime (hereafter the “horizontal” regime) is characterized by broad thermal boundary layers. This is a simple consequence of the suppression of all flow in these layers (see fig. 13a) by the perturbation magnetic field. As a result the temperature profile in these boundary layers is linear. For example, equation (32) shows that in the top boundary layer  $\theta_0 = K(1 - z)$ . Since

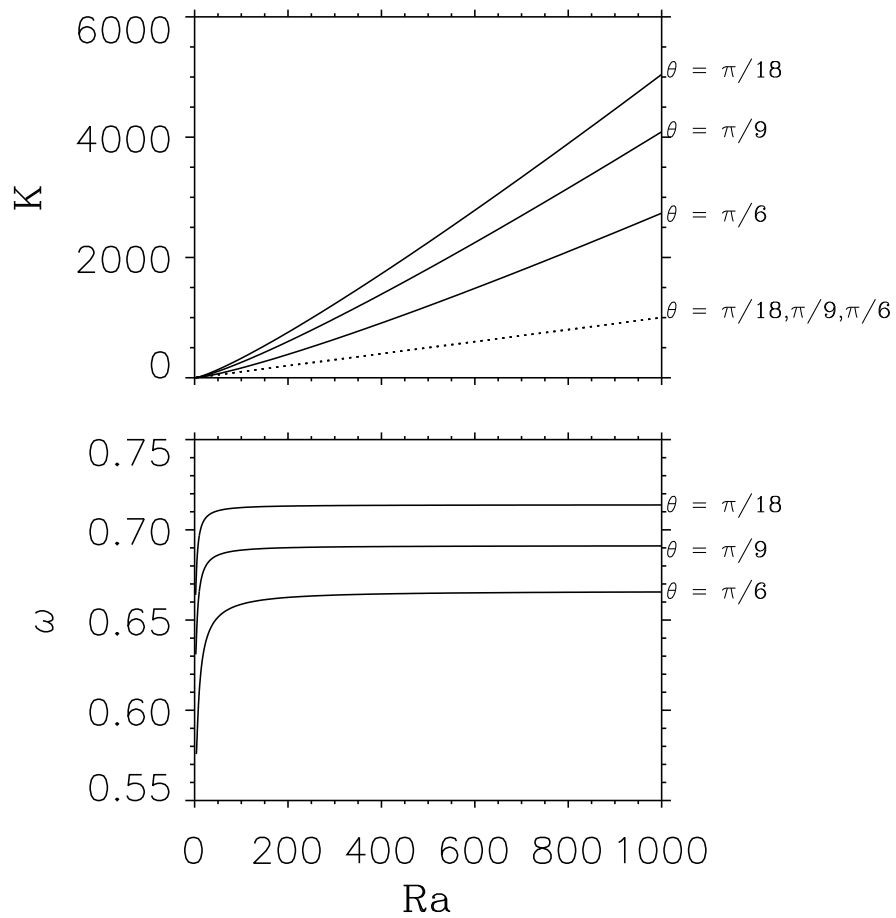


Figure 11: The (time-averaged) Nusselt number  $K$  for (a) steady (solid line) and oscillatory (dashed line) perpendicular rolls and  $\vartheta = 10^\circ, 20^\circ, 30^\circ$  as a function of the scaled Rayleigh number  $Ra$  when  $\zeta = 0.1$ ,  $\sigma = 1.1$ . Fig. (b) shows the corresponding oscillation frequency  $\omega$ .

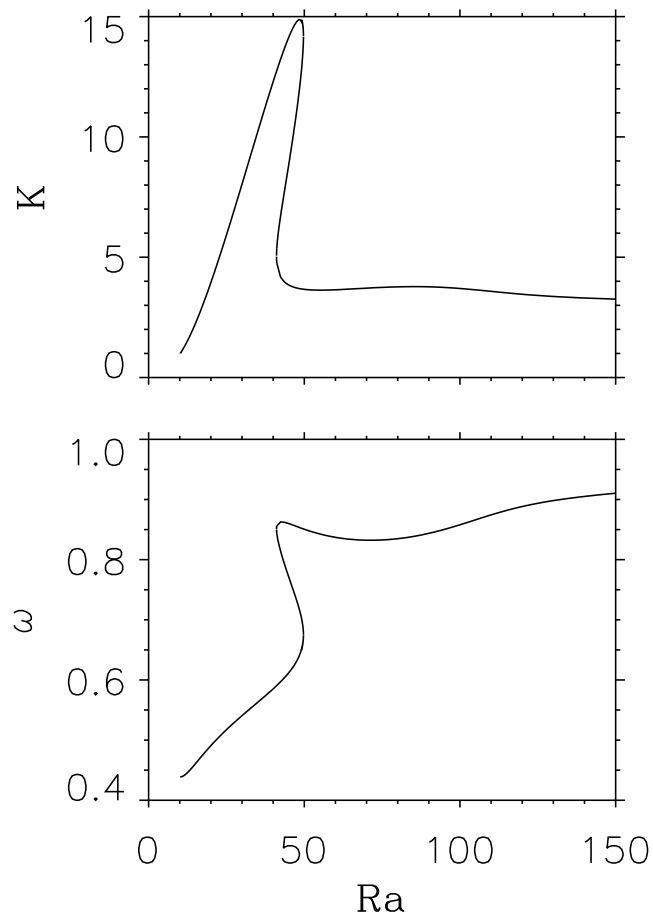


Figure 12: (a) The (time-averaged) Nusselt number  $K$  for oscillatory perpendicular rolls as a function of the scaled Rayleigh number  $Ra$  for  $\vartheta = \pi/4$  and  $\zeta = 0.1$ ,  $\sigma = 1.1$ . (b) The corresponding frequency  $\omega$ . Note the hysteretic transition from the “vertical” convection mode to the “horizontal” convection mode with increasing  $Ra$ .

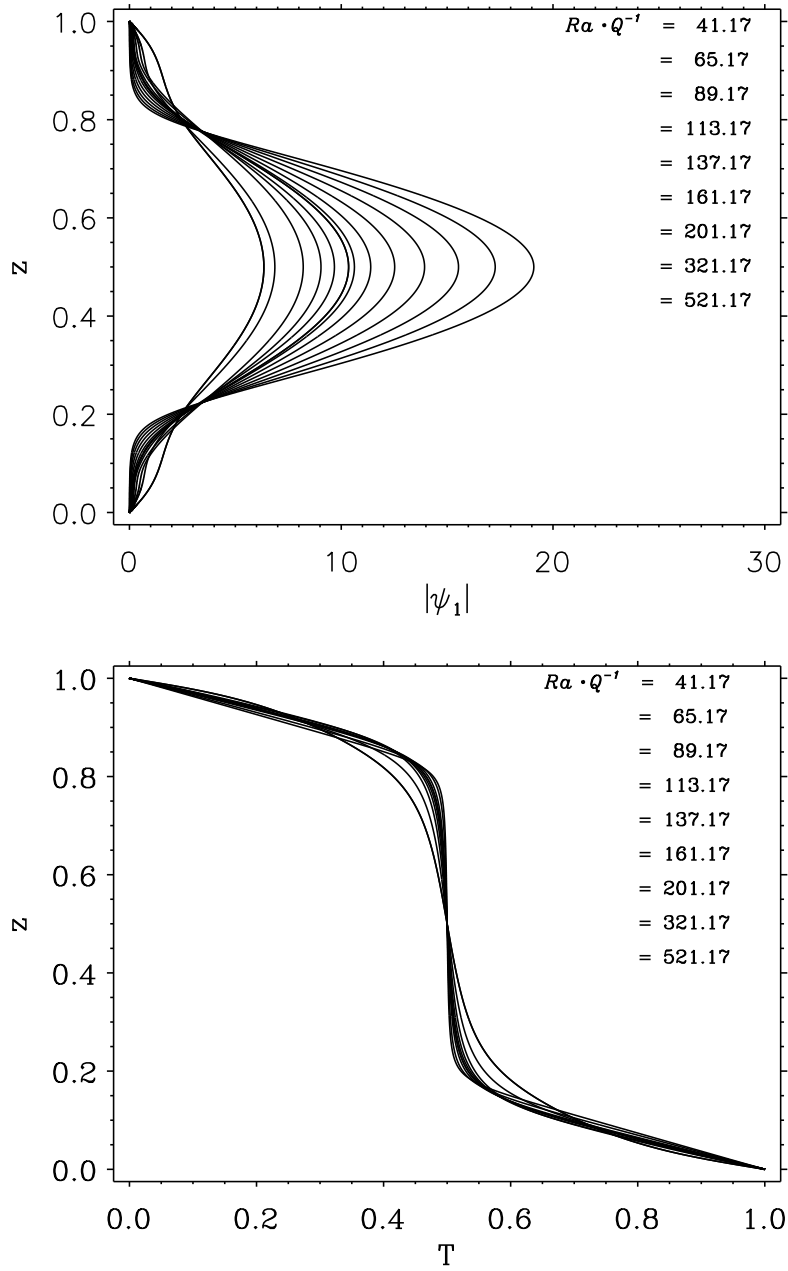


Figure 13: (a) Convection amplitude as measured by  $|\Psi(Z)|$  and (b) mean temperature profiles  $\theta_0(Z)$  for oscillatory perpendicular rolls at  $\vartheta = \pi/4$  at several values of the (scaled) Rayleigh number showing the development of broad boundary layers and small isothermal core with increasing  $Ra$  when  $\zeta = 0.1$ ,  $\sigma = 1.1$ . These properties are characteristic of the “horizontal” convection mode.

the temperature at the outer edge of the boundary layers is  $\theta_0 = 1/2$  their width is approximately  $1/2K$ . Moreover, since  $K$  is almost independent of the Rayleigh number so is their structure once the Rayleigh number is high enough. This is so despite the fact that the convective amplitude in the isothermal interior continues to increase as  $Ra^{1/2}$  in this regime. Note that the Rayleigh number must exceed a critical value before the “horizontal” convection mode sets in. This is because the flow in the interior must be strong enough to expell the magnetic field perturbation into the boundary layers at the top and bottom; this expulsion occurs primarily *along* the imposed magnetic field. In steady convection the resulting boundary layer thickness is determined by magnetic Reynolds number and is narrow if this is large. In contrast in oscillatory flow the flow reversals prevent the formation of such narrow boundary layers and the boundary layer thickness is determined by the perturbation Lorentz force rather than ohmic diffusion. The resulting boundary layers are therefore wider than in the case of steady convection. A number of conclusions follow immediately from the above considerations. First, the transition between the two regimes occurs at lower Rayleigh numbers when  $\vartheta$  is larger. Indeed for small values of tilt angle  $\vartheta$  we have shown that this transition to the lower “horizontal branch” does not occur (for this value of  $\zeta$ ) but that solutions stay on the efficient “vertical branch”. Moreover, since the ability of the magnetic field to suppress oscillatory convection increases with decreasing  $\zeta$  the value of the Rayleigh number at which the transition from the “vertical field” regime to the “horizontal field” regime takes place is an increasing function of  $\zeta$ . This argument also explains why the two convection regimes are only found in oscillatory convection.

In fig. 14 we show that if  $\zeta$  is increased too much (to  $\zeta = 0.15$  for this value of  $\vartheta$ ) the situation becomes radically different. The “vertical field” branch now extends to arbitrarily large Rayleigh numbers while the “horizontal field” branch has become disconnected. The upper saddle-node bifurcation has therefore disappeared. The disconnected branch moves away from the “vertical branch” as the tilt angle is decreased; moreover, the critical value of  $\zeta$  at which the vertical and horizontal field branches disconnect is an increasing function of  $\vartheta$ .

When  $\chi = \pi/2$  the behavior is similar but the “horizontal branch” appears only for larger values of  $\vartheta$ . Fig. 15 shows the Rayleigh number dependence of the Nusselt number and oscillation frequency for steady and oscillatory parallel rolls when  $\vartheta = 1$ ,  $\zeta = 0.1$  and  $\sigma = 1.1$ . Both convection modes are present at this tilt angle, in contrast to  $\vartheta = \pi/4$  for which the solutions remain on the “vertical branch” for all values of  $Ra$ , cf. fig. 12 for  $\chi = 0$ .

### 3.5 Tilted field with depth-dependent $\zeta$

The results for perpendicular rolls with  $\zeta(Z) = \zeta_0 + \epsilon(1 - Z)$  and  $\vartheta = \pi/4$  are shown in fig. 16. The behaviour of both the Nusselt number and frequency with increasing  $Ra$  is very similar to that in the vertical case. For the present parameter values the primary bifurcation is a steady state one but the resulting steady

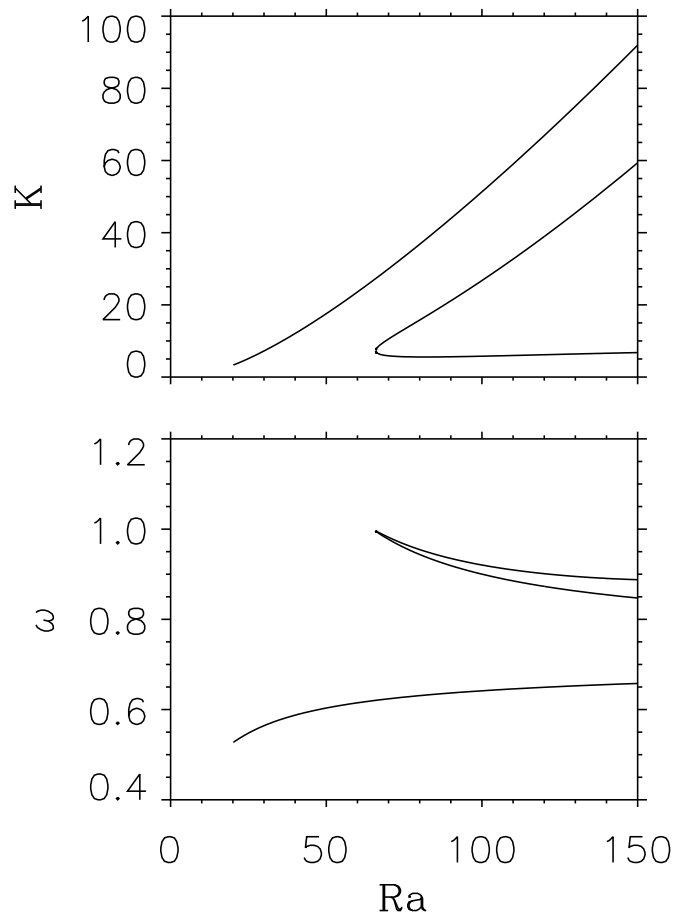


Figure 14: (a) The (time-averaged) Nusselt number  $K$  for oscillatory perpendicular rolls as a function of the scaled Rayleigh number  $Ra$  for  $\vartheta = \pi/4$  and  $\zeta = 0.15$ ,  $\sigma = 1.1$ , showing multiple branches. (b) The corresponding frequencies  $\omega$ .

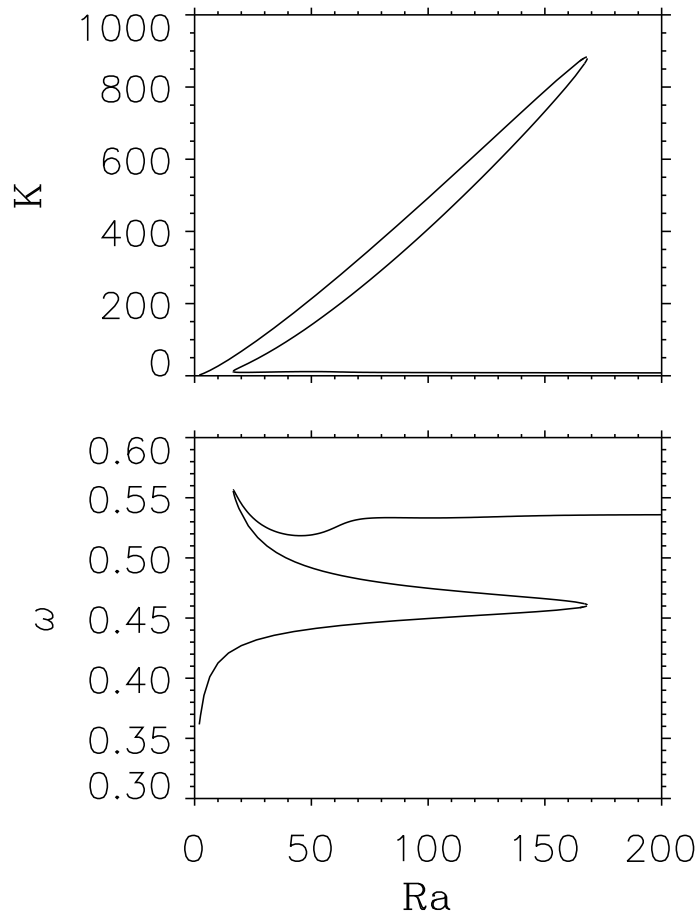


Figure 15: (a) The (time-averaged) Nusselt number  $K$  for steady (dashed line) and oscillatory (solid line) parallel rolls as a function of the scaled Rayleigh number  $Ra$  for  $\vartheta = 1$  when  $\zeta = 0.1$ ,  $\sigma = 1.1$ . Fig. (b) shows the corresponding (scaled) oscillation frequency  $\omega$ . There is no transition to the “horizontal” convection mode.

convection loses stability almost immediately in a Takens-Bogdanov bifurcation to an oscillatory mode. As  $Ra$  is increased further the oscillatory mode behaves in the usual manner for the “vertical branch” with  $K$  increasing monotonically with  $Ra$  and the frequency  $\omega$  saturating. Because of the up-down asymmetry introduced by the depth dependence of  $\zeta$ , the solution is no longer symmetric with respect to  $Z = 1/2$ . For these parameter values the depth dependence postpones the appearance of the “horizontal branch” to larger tilt angles.

## 4 Generalizations

The procedure outlined above can be generalized to astrophysically more realistic situations. We describe here some of these generalizations.

### 4.1 Newton’s law of cooling at the top

If instead of a fixed temperature boundary condition at the top we use the more realistic the boundary condition

$$D\theta_0 + \beta\theta_0 = 0 \text{ on } z = 1, \quad \beta > 0, \quad (48)$$

integration of equation (32) yields

$$K^{-1} = \left[ \int_0^1 \frac{\omega^2 + k_0^4}{\omega^2 + k_0^4 + 2k_0^2 k_{0\perp}^4 |\Psi|^2} dZ \right] + \beta^{-1}. \quad (49)$$

Thus

$$K^{-1} = K'^{-1} + \beta^{-1}, \quad (50)$$

where  $K'$  is the Nusselt number for fixed temperature boundary conditions. This result demonstrates that Newton’s law of cooling *reduces* the heat transport.

### 4.2 Fixed heat flux at top and bottom

If instead we impose fixed heat flux boundary conditions at both top and bottom

$$D\theta_0 = -F \text{ on } z = 0, 1, \quad (51)$$

then  $K = 1$  regardless of the value of the Rayleigh number. This simply states that whatever flux goes into the layer must also leave the layer. In this case the Nusselt number is clearly not a useful measure of the amplitude of convection. Instead the eigenvalue problem (34) becomes a nonlinear eigenvalue problem for  $Ra$  and  $\omega$  and we may use the kinetic energy  $E \equiv (1/2V) \int |\mathbf{u}|^2 dV$  as a suitable measure of the amplitude of convection. Thus no new calculations are necessary to solve the fixed flux problem. In general, an important feature of fixed flux convection is the selection of large scales at onset (Chapman and Proctor 1980,

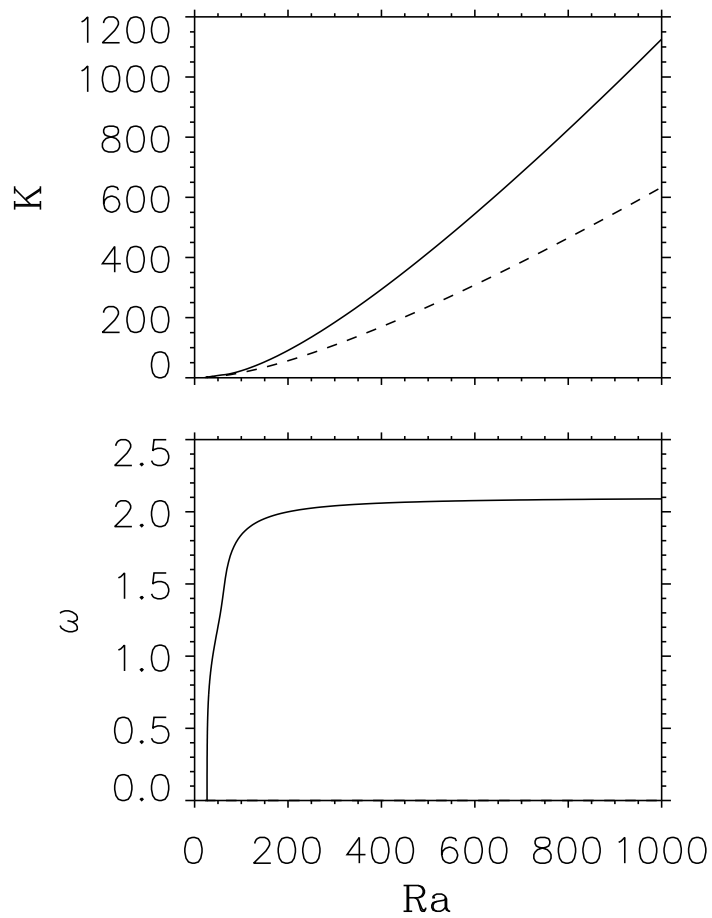


Figure 16: The (time-averaged) Nusselt number for oscillatory perpendicular rolls when  $\vartheta = \pi/4$  and  $\zeta(Z) = \zeta_0 + \epsilon(1 - Z)$  with  $\zeta_0 = 0.1$  and  $\epsilon = 2.0$ . (b) The corresponding frequency  $\omega(Ra)$ . The primary instability is a steady state one but the resulting steady convection loses stability almost immediately to oscillations.

Depassier and Spiegel 1981). If this were the case for magnetoconvection in the large  $Q$  limit the scaling employed in the derivation would be violated. Fig. 17 shows that this concern is unfounded. Although the selected wavenumber remains zero for sufficiently small  $Q$  it becomes finite for larger  $Q$  and rapidly approaches  $\mathcal{O}(Q^{\frac{1}{6}})$  values as in the case of fixed temperature boundaries. Moreover, in this regime the critical Rayleigh number increases as  $Q$ , as assumed in the theory.

The transition from zero to finite wavenumber with increasing  $Q$  is of interest in its own right and can be analyzed as in Knobloch (1989).

### 4.3 Magnetoconvection in a stratified atmosphere

Background stratification is not only important for astrophysical applications but also provides another source of vertical asymmetry. In such circumstances we expect qualitatively similar results to those found for depth-dependent  $\zeta$ . In this section we describe an analogous derivation for this case but confine attention to the simpler two-dimensional problem in an imposed vertical field. We eliminate sound waves using the magneto-anelastic approximation (Gilman and Glatzmaier 1981, Lantz and Sudan 1995) and thereby focus on dynamics on timescales long compared with the sound travel time. The basic state is described by the equations

$$\frac{dp_0}{dz} = -g\rho_0, \quad p_0 = \mathcal{R}\rho_0 T_0, \quad S_0 = \text{constant}. \quad (52)$$

Here  $\mathcal{R}$  is the gas constant. It follows from the first law of thermodynamics that

$$\frac{dT_0}{dz} = -\frac{g}{c_p} \quad (53)$$

and hence that

$$T_0 = T_s \left(1 - \frac{z}{h}\right), \quad \rho_0 = \rho_s \left(1 - \frac{z}{h}\right)^m, \quad p_0 = p_s \left(1 - \frac{z}{h}\right)^{m+1}, \quad (54)$$

where the subscript  $s$  denotes a reference value (at  $z = 0$ ),  $m$  is the polytropic index and  $h$  is the (temperature) scale height:

$$m = \frac{1}{\gamma - 1}, \quad h = \frac{c_p T_s}{g}. \quad (55)$$

Here  $\gamma = c_p/c_v$ .

In the following we discuss strongly nonlinear convection in such an atmosphere. The convection arises as a result of a buoyancy force due to a density perturbation  $\rho_1$  of the basic state  $\rho_0(z)$  assumed to be small compared to  $\rho_0$  but still large enough to drive fully nonlinear convection. The basic equations are

$$\rho_0 \frac{D\mathbf{u}}{Dt} = -\nabla p_1 - \rho_1 g \hat{\mathbf{z}} + \frac{1}{\mu_0} (\nabla \times \mathbf{B}) \times \mathbf{B} + \nabla \cdot \boldsymbol{\tau}, \quad (56)$$

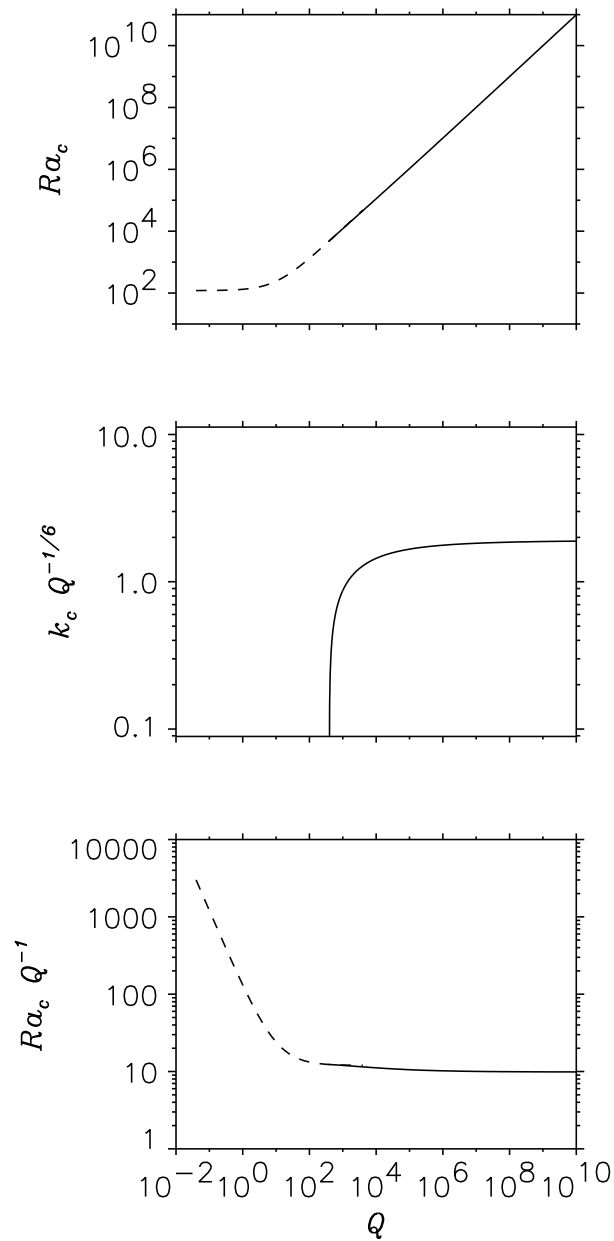


Figure 17: Linear theory results for onset of steady convection in a vertical magnetic field with fixed heat flux boundary conditions, showing that for sufficiently large  $Q$   $\mathcal{O}(Q^{1/6})$  wavenumbers are selected. The selected wavenumber  $k_c$  vanishes for  $Q < 376.5$  (theory predicts that the selected wavenumber vanishes at  $Q = Q_\infty = 376$ )

together with the continuity equation

$$\nabla \cdot \rho_0 \mathbf{u} = 0, \quad (57)$$

the entropy equation

$$\rho_0 T_0 \frac{DS_1}{Dt} = \nabla \cdot (\kappa \nabla T_1) + \frac{\eta}{\mu_0} |\nabla \times \mathbf{B}|^2 + \tau_{ij} \partial_j u_i, \quad (58)$$

and the induction equation

$$\frac{\partial \mathbf{B}}{\partial t} = \nabla \times (\mathbf{u} \times \mathbf{B}) - \nabla \times (\zeta \nabla \times \mathbf{B}), \quad \nabla \cdot \mathbf{B} = 0. \quad (59)$$

Here the subscripts 0,1 denote the basic state and the perturbation about it, respectively, and  $\mathbf{u}$ ,  $p$ ,  $\rho$ ,  $T$  and  $S$  are the velocity field, pressure, density, temperature and entropy per unit mass. In addition  $\mathbf{B}$  is the magnetic field while  $\tau$  is the viscous part of the stress tensor:  $\tau_{ij} = \mu(\partial_i u_j + \partial_j u_i - \frac{2}{3} \nabla \cdot \mathbf{u} \delta_{ij})$ , where  $\mu$  is the (possibly depth-dependent) coefficient of dynamic viscosity; bulk viscosity is neglected. The equations are complemented by the perturbed equation of state

$$\frac{\rho_1}{\rho_0} = \frac{p_1}{p_0} - \frac{T_1}{T_0}, \quad (60)$$

and the thermodynamic relation

$$S_1 = c_p \frac{T_1}{T_0} - \mathcal{R} \frac{p_1}{p_0}, \quad (61)$$

valid for  $p_1 \ll p_s$ ,  $\rho_1 \ll \rho_s$ ,  $T_1 \ll T_s$ .

To obtain results analogous to (34) it suffices to consider two-dimensional motions (see sect. 2). We therefore write

$$\rho_0 \mathbf{u} = \left( \frac{\partial \psi}{\partial z}, 0, -\frac{\partial \psi}{\partial x} \right), \quad \mathbf{B} = \left( \frac{\partial A}{\partial z}, 0, -\frac{\partial A}{\partial x} \right). \quad (62)$$

The resulting equations are nondimensionalized using a characteristic thermal diffusivity  $K_s$  (cm<sup>2</sup>/sec) to define units of time and velocity. We choose the layer depth  $d$  as unit of length and  $B_0$  as the unit of the magnetic field strength. The background pressure, density and temperature are scaled with  $p_s \equiv \mathcal{R} \rho_s T_s$ ,  $\rho_s$  and  $T_s$ . The thermodynamic relations become

$$\frac{\rho_1}{\rho_0} = -\frac{\Delta T \rho_s}{T_s \Delta \rho} \left( \frac{T_1}{T_0} - \frac{\Delta p}{\Delta T \mathcal{R} \rho_s} \frac{p_1}{p_0} \right), \quad S_1 = \frac{T_1}{T_0} - \left( 1 - \frac{1}{\gamma} \right) \frac{\Delta p}{\Delta T \mathcal{R} \rho_s} \frac{p_1}{p_0}, \quad (63)$$

where  $\Delta p$ ,  $\Delta \rho$  and  $\Delta T$  are the units used to nondimensionalize  $p_1$ ,  $\rho_1$  and  $T_1$ . The entropy  $S_1$  has been expressed in units of  $c_p \Delta T / T_s$ . Since the equation of motion indicates that the appropriate unit of  $p_1$  is the pressure  $\Delta p \equiv \rho_s K_s^2 / d^2$  we see that

$$\frac{\Delta p}{\Delta T \mathcal{R} \rho_s} = \frac{d}{h} \frac{\gamma}{\gamma - 1} Ra^{-1} \quad (64)$$

where

$$Ra = \frac{g\Delta T d^3}{K_s^2 T_s}, \quad Q = \frac{B_0^2 d^2}{\mu_0 \rho_s K_s^2}. \quad (65)$$

These definitions should be compared with (5). In the following we shall be interested in  $d/h = \mathcal{O}(1)$ ,  $Ra = \mathcal{O}(Q)$ . Consequently

$$s_1 = \frac{T_1}{T_0} + \mathcal{O}(Q^{-1}), \quad \frac{\rho_1}{\rho_0} = -\frac{\Delta T \rho_s T_1}{T_s \Delta \rho T_0} + \mathcal{O}(Q^{-1}) \quad (66)$$

and we do not have to calculate the pressure perturbation  $p_1$ . This offers a considerable simplification of the resulting equations which are

$$\begin{aligned} \nabla^2 \psi_t + \frac{1}{\rho_0} \psi_z \nabla^2 \psi_x &- \psi_x \nabla^2 \frac{\psi_z}{\rho_0} + 2 \frac{d}{h} \frac{\rho_{0z}}{\rho_0^2} \psi_x \psi_{xx} = -Ra \frac{\rho_0}{T_0} T_{1x} + Q (A_z \nabla^2 A_x - A_x \nabla^2 A_z) \\ &+ \left[ 2\sigma \left( \frac{\psi_{xz}}{\rho_0} + \frac{\partial}{\partial z} \frac{\psi_x}{\rho_0} \right) \right]_{xz} - (\partial_{xx} - \partial_{zz}) \sigma \left( \frac{\partial}{\partial z} \frac{\psi_z}{\rho_0} - \frac{\psi_{xx}}{\rho_0} \right), \end{aligned} \quad (67)$$

$$\begin{aligned} \rho_0 T_{1t} + \psi_z T_{1x} - \psi_x T_0 \frac{\partial}{\partial z} \left( \frac{T_1}{T_0} \right) &= \nabla \cdot \kappa \nabla T_1 + \frac{\zeta Q d}{Ra h} (\nabla^2 A)^2 + \frac{\sigma}{Ra \rho_0^2 h} \left[ \left( 2\psi_{xz} - \frac{\rho_{0z}}{\rho_0^2} \psi_x \right)^2 \right. \\ &\left. + \left( \psi_{xx} - \psi_{zz} + \frac{\rho_{0z}}{\rho_0^2} \psi_z \right)^2 + \frac{1}{3} \left( \frac{\rho_{0z}}{\rho_0^2} \psi_x \right)^2 \right], \end{aligned} \quad (68)$$

$$A_t + \frac{1}{\rho_0} \psi_z A_x - \frac{1}{\rho_0} \psi_x A_z = \zeta \nabla^2 A. \quad (69)$$

Here  $\zeta(z) = \eta(z)/K_s$ ,  $\sigma(z) = \mu/\rho_s K_s$  and  $\kappa(z)$  has been expressed in units of  $\rho_s c_p K_s$ .

Equations (67-69) form the basis for the subsequent study. We observe that these equations admit an equilibrium with a uniform vertical magnetic field and therefore write  $A \rightarrow -x + A$  so that nonzero  $A$  now indicates departure from the uniform vertical field. Since the imposed field is vertical the solutions vary on an  $\mathcal{O}(1)$  vertical scale only. Consequently, we set (cf. equation (9)):

$$\partial_x = Q^{\frac{1}{4}} \partial_{x'}, \quad \partial_z = D, \quad \partial_t = Q^{\frac{1}{2}} \partial_{t'}, \quad A = Q^{-\frac{1}{2}} A', \quad Ra = Q Ra' \quad (70)$$

and do not scale  $\psi$ . In addition we expand (dropping primes) the temperature in the form

$$T_1(x, z, t) = T_{10}(z) + Q^{-\frac{1}{4}} T_{11}(x, z, t) + Q^{-\frac{1}{2}} T_{12}(x, z, t) + \dots \quad (71)$$

Proceeding as in section 2 we obtain at leading order

$$\psi_{xt} = -Ra \frac{\rho_0}{T_0} T_{11} + D A_x + \frac{\sigma}{\rho_0} \psi_{xxx}, \quad (72)$$

$$A_t = \frac{D\psi}{\rho_0} + \zeta A_{xx} \quad (73)$$

$$\rho_0 T_{11t} - \psi_x T_0 D\left(\frac{T_{10}}{T_0}\right) = \kappa T_{11xx}. \quad (74)$$

The solvability condition for  $T_{12}$  yields

$$D(\kappa DT_{10}) = -D(\overline{\psi_x T_{11}}) + \overline{\psi_x T_{11}} \frac{DT_0}{T_0} - \frac{\zeta}{Ra} \frac{d}{h} \overline{A_{xx}^2} - \frac{\sigma}{Ra\rho_0^2} \frac{d}{h} \overline{\psi_{xx}^2}. \quad (75)$$

For solutions of the form (27) we find that  $\Psi(z)$  satisfies the nonlinear eigenvalue problem

$$D\left[\frac{D\Psi}{\rho_0(i\omega + \zeta k^2)}\right] - \left(i\omega + \frac{\sigma k^2}{\rho_0}\right)\Psi - Ra \frac{D(T_{10}/T_0)}{i\omega + (\kappa/\rho_0)k^2} \Psi = 0 \quad (76)$$

$$\begin{aligned} D(\kappa DT_{10}) = & - \frac{1}{2} \kappa k^4 \left\{ \frac{|\Psi|^2 T_0 D(T_{10}/T_0)}{\rho_0^2 \omega^2 + \kappa^2 k^4} \right\} + \frac{1}{2} \kappa k^4 \frac{|\Psi|^2 DT_0 D(T_{10}/T_0)}{\rho_0^2 \omega^2 + \kappa^2 k^4} \\ & - \frac{1}{2} \frac{\zeta}{Ra} \frac{d}{h} \frac{k^4 |D\Psi|^2}{\rho_0^2 (\omega^2 + \zeta^2 k^4)} - \frac{1}{2} \frac{\sigma}{Ra\rho_0^2} \frac{d}{h} k^4 |\Psi|^2. \end{aligned} \quad (77)$$

In these expressions

$$T_0 = T_s \left(1 - \frac{d}{h} z\right), \quad \rho_0 = \rho_s \left(1 - \frac{d}{h} z\right)^m, \quad (78)$$

and  $D$  indicates derivatives with respect to  $z$ . Note that the mean temperature equation no longer has an integral; an integral exists only when  $d \ll h$ . In this limit one recovers the Boussinesq formulation.

The linear problem in the stratified case is recovered on setting  $\Psi = 0$  in the temperature equation. Then

$$DT_{10} = -N/\kappa, \quad N^{-1} = \int_0^1 \frac{dz}{\kappa}, \quad (79)$$

and the eigenvalue problem becomes *linear*. This problem is to be solved for the critical Rayleigh number  $Ra_c$  for the onset of instability and  $\omega$  its frequency for given profiles of  $\kappa$ ,  $\zeta$ ,  $\rho_0$  and  $T_0$ . The nonlinear problem then describes the evolution of the convection amplitude  $\Psi$  and the accompanying deformation of the mean temperature profile as  $Ra$  increases above  $Ra_c$  much as in section 2.

## 5 Implications for sunspots

In this article we have summarized some of the fully nonlinear results that can be obtained by reformulating the problem of convection in an imposed magnetic

field as a nonlinear eigenvalue problem. Such a reformulation is possible when the field strength is large and the distortion of the field by the flow remains small. This reformulation promises to have significant applications in astrophysics and in particular for convection in sunspots, because realistic profiles of density and of the various diffusivities can be readily incorporated. We have considered here only the case where  $\zeta$  varies linearly with height, decreasing upwards, but considered both vertical and oblique magnetic fields. This choice of  $\zeta$  variation was motivated by the numerical simulations of two-dimensional compressible magnetoconvection in  $m = 1$  polytropic atmospheres with imposed vertical field by Weiss and colleagues. We have presented explicit results for incompressible convection, but have indicated how our procedure generalizes to the more realistic anelastic case. We have found that at large Rayleigh numbers the incompressible system develops an isothermal core just as in the case of constant  $\zeta$  except that the core temperature shifts away from  $T = 1/2$  and that the maximum amplitude of convection is displaced from midlevel. We have also seen that in overstable convection the dependence on the nonuniformity in  $\zeta$ , as parametrized by the parameter  $\epsilon$ , is nontrivial due to two competing effects. First, the assumed  $\zeta$  variation tends to localize the oscillations towards the upper boundary. At the same time, however, it tends to raise the value of  $\zeta$  at midlevel and hence to suppress oscillations altogether. We found, moreover, that when the field is inclined the behaviour of the overstable system falls into one of two possible regimes. For small tilt angles the magnetic field plays a minor role in inhibiting convection and the Nusselt number is an increasing function of the Rayleigh number. If the tilt angle is increased past a threshold value (which depends on the value of  $\zeta$  and on the roll orientation  $\chi$ ) a hysteretic transition takes place with increasing Rayleigh number from this “vertical field” regime to a “horizontal field” regime in which the field plays a major role in inhibiting the heat transport. Detailed results demonstrating this behaviour were presented for both perpendicular and parallel rolls. Although we have been unable to verify that this novel convection regime persists for the (smaller) wavenumbers selected by linear theory for perpendicular rolls at large  $Q$  at these tilt angles, for parallel rolls the selected wavenumbers remain large and the asymptotic theory captures correctly both convection regimes. Continuity arguments suggest that in the absence of secondary Hopf and parity-breaking bifurcations (and of sideband instabilities) the “vertical field” branch will be stable up to the first saddle-node bifurcation (if present), as will the “horizontal field” branch beyond the second saddle-node bifurcation; the branch between the two saddle-nodes is expected to be unstable. These expectations will be checked using direct numerical simulations of the reduced equations.

It is tempting to speculate about the possible role of the fully nonlinear solutions discovered here for the structure of a sunspot. Sunspots consist of a dark central region, the umbra, surrounded by a non-axisymmetric filamentary penumbra. The penumbra is characterised by radial striations of alternating bright and

dark filaments. The reason for the sudden transition between the umbra and the penumbra is poorly understood – but the nonlinear results discussed above suggest a possible mechanism. Observations have shown (e.g., Title *et al.* 1992) that the magnetic field strength does not change significantly across the spot, although the tilt angle does. In the sunspot umbra the magnetic field is nearly vertical, while in the penumbra it is tilted, with the tilt angle away from the vertical an increasing function of distance from the centre. Danielson (1961) in his study of tilted magnetoconvection speculated that the gradual change in tilt angle would lead to a change in the nature of convection from three-dimensional to two-dimensional but did not explain why the transition should be so abrupt. The results described in this paper suggest a possible scenario (see figs. 18, 19). For small tilt angles the system shows little preference between parallel and perpendicular rolls and the convection is expected to be fully three-dimensional. [For vertical magnetic fields the results of Clune & Knobloch (1993) indicate that, in the weakly nonlinear regime, three-dimensional structures are preferred at large  $Q$  if the onset of convection is oscillatory]. Moreover, both parallel and perpendicular rolls remain on the vertical field branch as the tilt angle is increased (at fixed supercritical  $Ra$ ) and both transport energy efficiently. We have seen, however, that there is a critical tilt angle  $\vartheta_c$  at which there is a saddle-node bifurcation beyond which the system settles onto the horizontal field branch (fig. 19). Although such a saddle-node bifurcation is present for both perpendicular and parallel rolls it is encountered first for the perpendicular rolls as  $\vartheta$  (or, equivalently, the radial distance from the spot centre) increases. As described above, convection on the horizontal field branch is very inefficient and for  $\vartheta > \vartheta_c$  the Nusselt number drops to small values. This argument suggests that for  $\vartheta > \vartheta_c$  heat will be transported only by parallel (i.e., radial) rolls which continue to be efficient transporters of heat; we suppose these to be in the form of *standing* waves. Although this argument ignores the nonlinear nature of the solutions at supercritical Rayleigh numbers it does provide a natural and promising explanation for the observed sharp transition from three-dimensional to two-dimensional radial structures observed in sunspots. Moreover, it has much in common with the sunspot model put forward recently by Rucklidge *et al.* (1995). In particular figs. 18, 19 suggest that when  $Ra = 100$  the transition to a penumbra occurs at  $\vartheta \approx 0.66$  but is absent for  $Ra = 45$ , i.e., the penumbra develops with increasing  $Ra$ . The same argument suggests that the second transition, at  $\vartheta \approx 1$ , should be associated with the appearance of a new mode of convection, presumably field-free convection outside the spot. It is of interest that the tilt angle of the field at the outer edge of the penumbra of a typical sunspot is  $\approx 70^\circ$ .

The scenario outlined above competes with an additional effect due to the variation of the effective Rayleigh number across the spot. If we suppose that the temperature difference between some reference depth and the surface remains constant across the spot and that the temperature at depth is uniform, the imposed

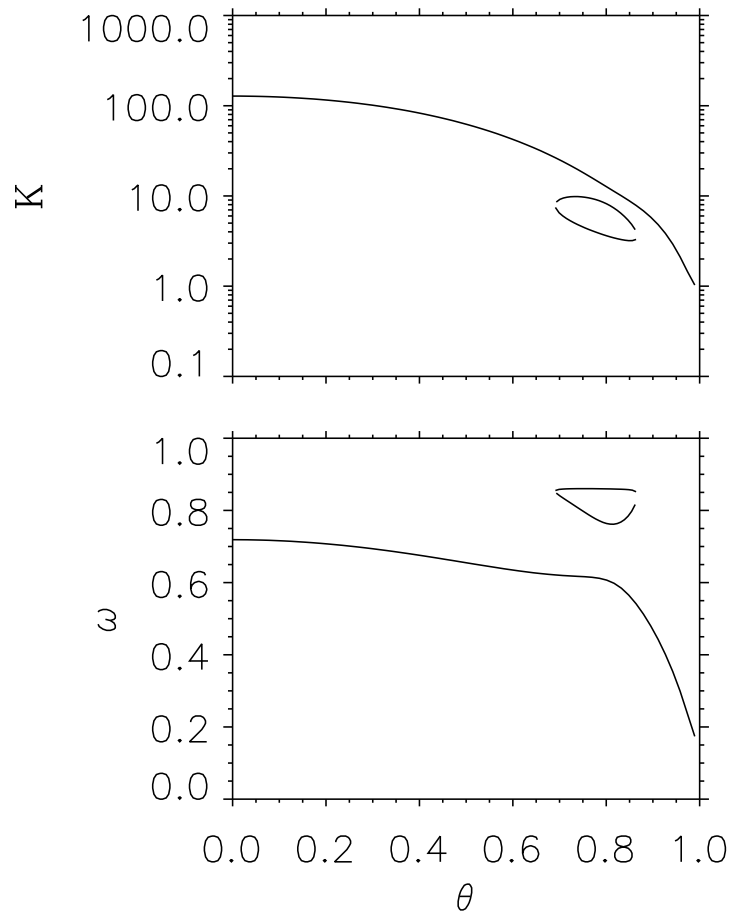


Figure 18: (a) The (time-averaged) Nusselt number for oscillatory perpendicular rolls as a function of the tilt angle  $\vartheta$  when  $Ra = 45$ ,  $\zeta = 0.1$ ,  $\sigma = 1.1$ . (b) The corresponding frequency  $\omega(Ra)$ . Note the presence of an isola of solutions; of these those above and between the two saddle-node bifurcations are expected to be stable.

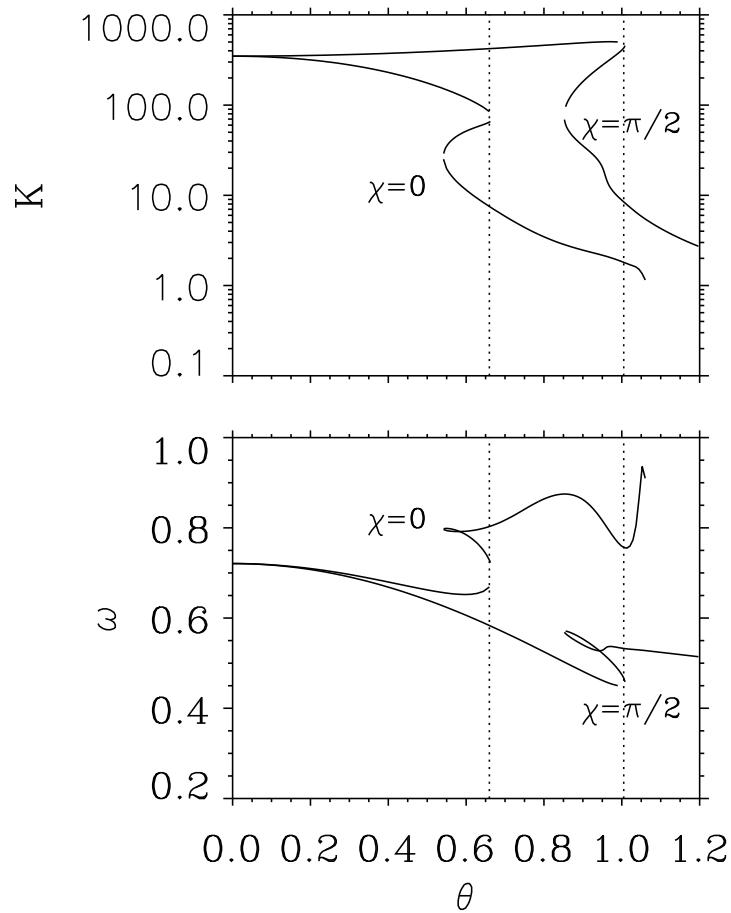


Figure 19: (a) Same as fig. 18(a) but for both perpendicular ( $\chi = 0$ ) and parallel ( $\chi = \pi/2$ ) rolls when  $Ra = 100$ . (b) The corresponding frequency  $\omega(Ra)$ . The transition to the inefficient “horizontal mode” occurs first for the perpendicular rolls and defines the critical tilt angle  $\vartheta_c$ .

Rayleigh number  $Ra$  will be constant across the spot. In this case Nusselt number variations across the spot (see figs. 18, 19) do not translate into variations in temperature at the visible surface ( $\tau = 1$  depth). However, linear theory shows that at large  $Q$  the critical Rayleigh number  $Ra_c$  steadily decreases as the tilt angle increases (fig. 2), so that the supercriticality, or *effective* Rayleigh number, increases with radial distance from the spot centre. Although this property of the exact linear problem is absent in the asymptotic regime considered here it suggests that we identify our low Rayleigh number “vertical mode” results with convection in the umbra, and our higher Rayleigh number “horizontal mode” results with convection in the penumbra. In this scenario the saddle-node bifurcation is again responsible for the abrupt change in the properties of the umbra and penumbra even though the effective Rayleigh number may vary gradually across the spot.

The  $K(Ra)$  plots in figs. 12, 14 and the  $K(\vartheta)$  plots in fig. 19 suggest what might happen if we instead imagine fixing the heat flux  $K$  (cf. Busse 1967) rather than fixing  $Ra$ . Fig. 12 shows that there may be as many as three values of  $Ra$  at which the (time-averaged) heat transport takes the desired value  $K$ , a stable one at low  $Ra$ , an unstable one in the middle, and another stable one at very large  $Ra$ ; the latter may not be present in the figure which examines only  $\mathcal{O}(Q)$  values of  $Ra$ , but must appear at larger  $Ra$ . This argument also argues in favour of a low  $Ra$  vertical field regime and a large  $Ra$  horizontal field regime, with an abrupt transition between the two; fig. 19 indicates that in a spot with a gradually varying angle of tilt these regimes would be spatially disjoint. Suitably reformulated, an argument of this type would allow an abrupt temperature change at the  $\tau = 1$  depth with increasing tilt angle, and could, combined with the first argument, describe a filamentary penumbra of the observed type.

## Acknowledgements

This work reported here was supported by NASA under SR&T grants NAG5-4918 and MASW-99026 (KJ), DOE under grant DE-FG03-95ER-25251 (EK), NSF under grant DMS-9703684 (EK) and NASA under SPTP grant NAG5-2256 (SMT).

## References

- [1] Busse, F. H. 1967 Non-stationary finite amplitude convection. *J. Fluid Mech.* **28**, 223–239.
- [2] Chandrasekhar, S. 1961 *Hydrodynamic and Hydromagnetic Stability*, Oxford University Press.
- [3] Chapman, C. J. and Proctor, M. R. E. 1980 Nonlinear Rayleigh-Bénard convection between poorly conducting boundaries. *J. Fluid Mech.* **101**, 759–782.

- [4] Clune, T. and Knobloch, E. 1993 Pattern selection in three-dimensional magnetoconvection. *Physica D* **74**, 151–176.
- [5] Danielson, R. E. 1961 The structure of sunspot penumbras. II. Theoretical. *Astrophys. J.* **134**, 289–311.
- [6] Depassier, M. C. and Spiegel, E. A. 1981 The large-scale structure of compressible convection. *Astron. J.* **86**, 496–512.
- [7] Gilman, P. A. and Glatzmaier, G. A. 1981 Compressible convection in a rotating spherical shell. I. Anelastic equations. *Astrophys. J. Suppl.* **45**, 335–349.
- [8] Hughes, D. W. and Proctor, M. R. E., 1988 Magnetic fields in the solar convection zone. *Ann. Rev. Fluid Mech.* **20**, 187–223.
- [9] Julien, K. and Knobloch, E. 1998 Strongly nonlinear convection cells in a rapidly rotating fluid layer: the tilted  $f$ -plane. *J. Fluid Mech.* **360**, 141–178.
- [10] Julien, K., Knobloch, E. and Tobias, S. M. 1999 Strongly nonlinear magnetoconvection in three dimensions. *Physica D* **128**, 105–129.
- [11] Julien, K., Knobloch, E. and Tobias, S. M. 2000 Nonlinear magnetoconvection in the presence of strong oblique fields. *J. Fluid Mech.* **410**, 285–322.
- [12] Julien, K., Knobloch, E. and Werne, J. 1998 A new class of equations for rotationally constrained flows. *Theor. Comp. Fluid Dyn.* **11**, 251–261.
- [13] Knobloch, E. 1989 Pattern selection in binary-fluid convection at positive separation ratios. *Phys. Rev. A* **40**, 1549–1559.
- [14] Knobloch, E. 1994 Bifurcations in rotating systems, in *Lectures on Solar and Planetary Dynamos*, M. R. E. Proctor and A. D. Gilbert (eds.), Cambridge University Press, pp. 331–372.
- [15] Knobloch, E. and Weiss, N. O., 1984 Convection in sunspots and the origin of umbral dots. *Mon. Not. R. astr. Soc.* **207**, 203–214.
- [16] Lantz, S. R. and Sudan, R. N. 1995 Magnetoconvection dynamics in a stratified layer. I. Two-dimensional simulations and visualization. *Astrophys. J.* **441**, 903–924.
- [17] Matthews, P. C. 1999 Asymptotic solutions for nonlinear magnetoconvection. *J. Fluid Mech.*, **387**, 397–409.
- [18] Matthews, P. C., Hurlburt, N. E., Proctor, M. R. E. and Brownjohn, D. P. 1992 Compressible magnetoconvection in oblique fields: linearized theory and simple nonlinear models. *J. Fluid Mech.* **240**, 559–569.

- [19] Proctor, M. R. E., Weiss, N. O. 1982 Magnetoconvection. *Rep. Prog. Phys.* **45**, 1317–1379.
- [20] Rucklidge, A. M., Schmidt, H. U. and Weiss, N. O. 1995 The abrupt development of penumbrae in sunspots. *Mon. Not. R. astr. Soc.* **273**, 491–498.
- [21] Thomas, J. H. and Weiss, N. O. 1992 The theory of sunspots. In *Sunspots: Theory and Observations*, J. H. Thomas and N. O. Weiss (eds), Kluwer, pp. 3–59.
- [22] Title, A. M., Frank, Z. A., Shine, R. A., Tarbell, T. D., Topka, K. P., Scharmer, G., Schmidt, W. 1992 High resolution observations of the magnetic and velocity field of simple sunspots. In *Sunspots: Theory and Observations*, J. H. Thomas and N. O. Weiss (eds), Kluwer, pp. 195–219.
- [23] Weiss, N. O., Brownjohn, D. P., Hurlburt, N. E. and Proctor, M. R. E. 1990 Oscillatory convection in sunspot umbrae. *Mon. Not. R. astr. Soc.* **245**, 434–452.
- [24] Weiss, N. O., Brownjohn, D. P., Matthews, P. C. and Proctor, M. R. E. 1996 Photospheric convection in strong magnetic fields. *Mon. Not. R. astr. Soc.* **283**, 1153–1164.